

1 **The role of fault network geometry on the complexity of**  
2 **seismic cycles in the Apennines**

3 Constanza Rodriguez Piceda<sup>1,2</sup>, Zoë K. Mildon<sup>1</sup>, Billy J. Andrews<sup>1</sup>, Yifan ~~Yin~~<sup>3</sup>, Jean-Paul

4 ~~Ampuero~~<sup>4</sup>, Martijn van den ~~Ende~~<sup>4</sup>, Claudia ~~Sgambato~~<sup>5</sup>, Percy ~~Galvez~~<sup>6</sup>

5 <sup>1</sup> University of Plymouth, School of Geography, Earth and Environmental Sciences, Plymouth, PL4 8AA,  
6 United Kingdom

7 <sup>2</sup> GFZ Helmholtz Centre for Geosciences, Potsdam, ~~14473~~, Germany

8 <sup>3</sup> MIT Department of Earth, Atmospheric and Planetary Science, Cambridge, MA 02139, United States

9 <sup>4</sup> Université Côte d'Azur, Observatoire de la Côte d'Azur, IRD, CNRS, ~~Géo azur~~, Valbonne, 06905, France

10 <sup>5</sup> Birkbeck University of London, London, WC1E 7HX, United Kingdom

11 <sup>6</sup> Everest Group, Zürich, CH-8001, Switzerland

12 Correspondence to: [constanza.rodriguezpiceda@plymouth.ac.uk](mailto:constanza.rodriguezpiceda@plymouth.ac.uk)

13

Deleted: Yin<sup>2</sup>

Deleted: Ampuero<sup>3</sup>

Deleted: Ende<sup>3</sup>

Deleted: Sgambato<sup>4</sup>

Deleted: Galvez<sup>5</sup>

Formatted: Superscript

Formatted: Font: Not Bold

Deleted: <sup>2</sup>

Deleted: <sup>3</sup>

Deleted: Géoazur

Formatted: English (UK)

Deleted: <sup>4</sup>

Deleted: <sup>5</sup>

24 **Abstract.** Estimating the recurrence intervals and magnitudes of earthquakes for a given fault is essential for  
25 seismic hazard assessment but often challenging due to the long recurrence times of large earthquakes. Fault  
26 network geometry (i.e. spatial arrangement between faults) plays a key role in modulating stress interactions and,  
27 consequently, earthquake recurrence and magnitude. Here, we investigate these effects of fault network geometry  
28 using earthquake cycle models to generate numerous earthquakes on two different networks of normal faults in  
29 Italy: the Central Apennines, characterised by a wide network of faults offset across strike, and the Southern  
30 Apennines, a narrow fault network where faults are predominantly arranged along strike. For each region, we ran  
31 an earthquake cycle simulation on systems of seven normal faults generating approximately 150 earthquakes. In  
32 the Central Apennines, co-seismic stress transfer between faults promotes more heterogeneous stress, more partial  
33 ruptures, greater Mw variability and less periodic behaviour of large earthquakes (coefficient of variation of  
34 recurrence time, CV 0.1-0.9). In contrast, faults in the Southern Apennines experience more homogeneous stress  
35 loading, leading to a higher proportion of full-fault ruptures with more regular recurrence intervals (CV 0-0.4). In  
36 both fault networks, high long-term slip rate amplifies the effects of fault interactions: faults with higher long-  
37 term slip rate are more sensitive to positive stress perturbations from nearby faults compared to slower-moving  
38 faults. These results highlight that incorporating stress interactions from fault network geometry into seismic  
39 hazard models is particularly important for networks of faults offset across strike, where rupture behaviour is more  
40 variable.

## 41 1 Introduction

42 Earthquake recurrence intervals and magnitude distributions are key inputs for probabilistic and time-dependent  
43 seismic hazard assessment (Gerstenberger et al., 2020), therefore determining the mechanisms behind their  
44 variability is necessary to effectively mitigate associated risks. Fault stress interactions, which occur as stress is  
45 redistributed following earthquakes (Harris and Simpson, 1998; King et al., 1994; Stein, 1999), influence the  
46 recurrence and magnitude of earthquakes. These interactions can be either permanent (Coulomb static stress  
47 transfer, CST) or transient (associated with seismic wave propagation; Freed, 2005), and may either promote or  
48 inhibit rupture depending on the relative location and orientation of faults (e.g., Harris and Simpson, 1998; King  
49 et al., 1994; Nicol et al., 2005; Stein, 1999).

50 Several studies have investigated how fault network geometry shapes stress interactions (Cowie et al., 2012;  
51 Rodriguez Piceda et al., 2025a; Sgambato et al., 2020a, 2023). In particular, here we distinguish two basic spatial  
52 arrangements of fault networks: “along-strike fault networks” in which faults are co-planar, aligned in the along-  
53 strike direction, and “across-strike fault networks” in which faults are non-co-planar, offset in the across-strike  
54 direction. Sgambato et al. (2020, 2023) used CST analysis of historical earthquakes in Italy to show that faults  
55 with more across-strike interactions develop more irregular stress loading histories, less dominated by interseismic  
56 stress loading, whereas faults with fewer across-strike interactions tend to have more regular stress histories  
57 controlled by interseismic loading. While these patterns suggest a link between stress loading history and the  
58 regularity of earthquake recurrence, it remains difficult to isolate the effects of network geometry using historical  
59 data alone, since other processes such as dynamic stress transfer from seismic waves, postseismic stress  
60 redistribution and fluid pressure changes (Freed, 2005) can obscure stress patterns driven by network geometry.

Formatted: English (UK)

Formatted: English (UK)

Formatted: English (UK)

61 To explore the effects of network geometry under controlled conditions, numerical modelling approaches have  
62 been employed. For instance, studies with elastic-brittle lattice models (e.g., Cowie et al., 2012) found that more  
63 across-strike interactions lead to shorter earthquake recurrence intervals. However, these models do not include  
64 the effects of time-dependent stress healing and frictional memory as observed in natural fault rocks (Marone,  
65 1998b), resulting in less realistic stress-loading histories, nor they address the effects of fault geometry in  
66 earthquake magnitudes and the partition between seismic and aseismic slip modes.

67 These effects are accounted for in models of sequences of earthquakes and aseismic slip (SEAS), incorporating  
68 rate-and-state friction, enabling a more realistic representation of nucleation, healing and slip mode variability  
69 (Erickson et al., 2020; Jiang et al., 2022; Lapusta et al., 2000; Rice, 1993). For example, Romanet et al., (2018)  
70 modelled two partially overlapping strike-slip faults with equal long-term tectonic slip rate and found that smaller  
71 across-strike separations can produce complex earthquake sequences and slow slip events. Yin et al. (2023)  
72 extended this to three overlapping strike-slip faults, showing that fault interactions promote aperiodic cycles and  
73 partial ruptures (i.e. ruptures that do not break the whole fault). Rodriguez Picada et al., (2025a) focussed on the  
74 role of along-strike and across-strike separation on the earthquake cycle using a simplified system of two parallel  
75 normal faults with identical loading conditions. They showed that across-strike separation has a greater impact on  
76 recurrence intervals than along-strike separation, with closer across-strike faults characterised by more complex  
77 and non-periodic seismic cycles.

78 Natural fault networks, however, are geologically more complex than in generic models: they are often formed  
79 by more than three faults, are more geometrically diverse, and long-term slip rates vary between faults (e.g. Nicol  
80 et al., 2016; Papanikolaou et al., 2005; Papanikolaou and Roberts, 2007; Roberts, 2007; Roberts and Michetti,  
81 2004). The combined effect of such complexities on earthquake timing, magnitude and slip modes remains poorly  
82 understood, as does the role of slip rate in modulating interaction effects. These research gaps have direct  
83 implications for seismic hazard assessment.

84 Here we address these questions by introducing a novel approach developing 3D SEAS simulations of over 100  
85 earthquakes based on the Southern and Central Apennines normal-fault networks in Italy, an ideal natural  
86 laboratory due to its diverse network geometries and fault slip rates constrained by field data (Faure Walker et al.,  
87 2021; Mildon et al., 2019; Sgambato et al., 2020b) and exceptional historical and paleoseismic records (Galadini  
88 and Galli, 1996, 1999a; Galli et al., 2015; Galli, 2020; Guidoboni et al., 2019; Pantosti et al., 1993; Rovida et al.,  
89 2020). This approach overcomes several of the simplifications of previous studies by combining realistic fault  
90 network geometries, field-derived loading rates and spontaneous rupture propagation within a continuum  
91 framework. We investigate the effects of network geometry and long-term slip rate on earthquake recurrence,  
92 magnitude distributions, and slip behaviour, and discuss the implications for incorporating such variability into  
93 time-dependent seismic hazard models.

## 94 2 Geological background

95 The Apennines fold-and-thrust belt developed during the Neogene and Quaternary due to the convergence  
96 between the Eurasian and African plates (Anderson and Jackson, 1987; Doglioni, 1993; Jolivet et al., 1998). The  
97 thrusting phase was followed by extensional tectonics during the Pliocene (~2-3 Ma; Cavinato & Celles 1999;

Formatted: English (UK)

Formatted: English (UK)

Deleted: Rodriguez Picada et al. (2025)

Deleted: (

Deleted: ,

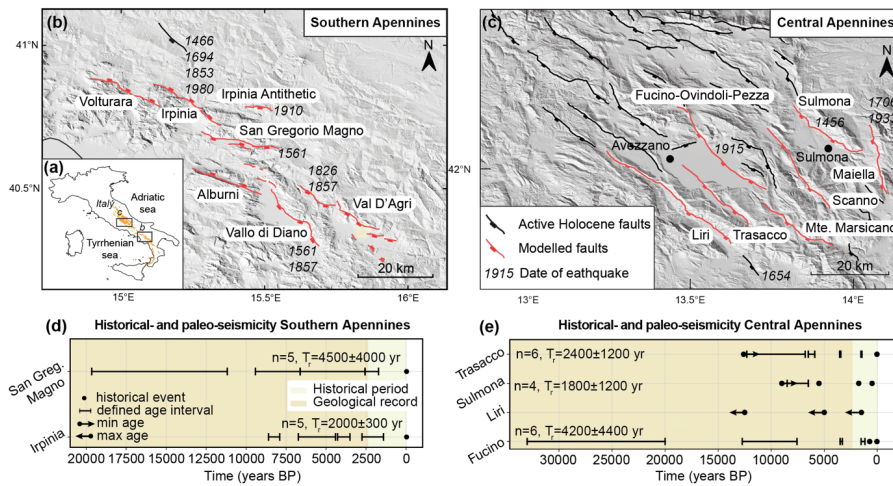
Deleted: {Citation}

Formatted: English (UK)

Formatted: English (UK)

102 Roberts & Michetti 2004). This extensional phase, continuing to the present day, led to the formation of NW-SE  
103 oriented normal faults that run nearly parallel to the fold-and-thrust belt. The tectonically active faults have formed  
104 surface offsets preserved since the Last Glacial Maximum (12-18 Ka), allowing the estimation of throw rates from  
105 exposed Holocene fault scarps (Papanikolaou and Roberts, 2007; Roberts and Michetti, 2004). In the Southern  
106 Apennines, average throw rates on individual faults range between 0.2 and 0.67 mm/yr (Faure Walker, 2010;  
107 Papanikolaou and Roberts, 2007; Roberts and Michetti, 2004; Sgambato et al., 2020a, b), while in the Central  
108 Apennines, they range between 0.2 and 1.56 mm/yr (Faure Walker et al., 2009; Faure Walker, 2010; Faure Walker  
109 et al., 2019a, 2021; Mildon et al., 2019; Papanikolaou and Roberts, 2007; Roberts and Michetti, 2004). The  
110 different slip rates among faults allowed us to assess how slip rates modulate or amplify stress transfer and  
111 interaction between faults.

112 A subset of faults in the Southern and Central Apennines was chosen for computational efficiency. The chosen  
113 fault networks differ in the number, length and orientation of faults. The chosen sector in the Central Apennines  
114 is characterised by a wide fault network, with up to 8 faults arranged NW-SE (Fig. 1b), whereas the Southern  
115 Apennines has a narrower fault network with fewer faults accommodating the extension, with a maximum of 3  
116 across-strike faults (Fig. 1c). These faults are associated with moderate to large magnitude earthquakes (Mw 5.5-  
117 7; e.g., Bagh et al., 2007; Chiaraluce et al., 2005, 2022; Guidoboni et al., 2019). In the Southern Apennines, the  
118 historical record documents 9 earthquakes of Mw>5.6 since 1466 associated with the studied faults (Fig. 1c, Table  
119 B1; Cello et al., 2003; Galli et al., 2006, 2014; Galli and Peronace, 2014; Giardini et al., 1996; Rovida et al., 2020;  
120 Westaway, 1993; Westaway and Jackson, 1987). Two multi-fault seismic sequences have occurred in the region:  
121 one in 1857 of estimated Mw 7.1 involving either the Vallo di Diano and the Val D'Agri faults (Benedetti et al.,  
122 1998; Cello et al., 2003; Galli et al., 2006a) or the Caggiano-Montemurro fault (Bello et al., 2022); and a second  
123 in 1980 of Mw 6.81 that ruptured the Irpinia (also known as Monte Marzano fault, e.g., Galli, 2020), and Irpinia  
124 antithetic faults, as well as possibly the San Gregorio fault (Sgambato et al., 2025). This rupture included a  
125 northeast dipping segment of the Irpinia fault known as the Pantano di San Gregorio segment (D'Adezzio et al.,  
126 1991, Fig. 1b). The 1980 event was the largest earthquake instrumentally recorded in the Apennines (Bernard and  
127 Zollo, 1989). In the studied segment of the Central Apennines, the historical record includes 7 earthquakes of  
128 Mw>5.6 since 1456 associated with the studied faults, including the 1915 A.D Fucino earthquake. Paleoseismic  
129 data is available for 1 and 4 of the modelled faults in Southern and Central Apennines, respectively (Fig. 1d-e,  
130 Table B2).



131

132 **Figure 1: (a) Location of selected fault regions in Italy; (b-c) Map of the fault regions in the Apennines and**  
 133 **historical earthquakes (post 1400AD). Active Holocene fault traces in the (b) Southern Apennines (based**  
 134 **on Sgambato et al., 2020b) and (c) Central Apennines (based on Faure Walker et al., 2021), showing the**  
 135 **different fault network geometries between the regions, with few across-strike faults in the Southern**  
 136 **Apennines and multiple across-strike faults for Central Apennines. Dashed black lines show the debated**  
 137 **link between Vallo di Diano and Auletta faults and Auletta and Caggiano-Montemurro faults (see section**  
 138 **3.1). (d-e) Chronology of paleoseismic and historical events with  $M > 6$  in modelled faults of the (d) Southern**  
 139 **Apennines and (e) Central Apennines (see Table B2 for details; Galadini and Galli, 1999a, a; Galli et al.,**  
 140 **2008, 2015, 2016; Pace et al., 2020; Pantosti et al., 1993). Whisker plots represent the estimated time range**  
 141 **of seismic events. The number of paleoseismic events per fault with defined aged brackets (n), and their**  
 142 **estimated mean and standard deviation of recurrence time ( $T_r$ ) is also shown.**

### 143 3 Methods

#### 144 3.1 Model set-up

145 We use the boundary-element software QDYN (Luo et al., 2017) to model SEAS on the Southern and Central  
 146 Apennines fault networks, each composed of 2D normal faults governed by rate-and-state friction, embedded in  
 147 a 3D elastic medium (see Appendix A for a description of the governing equations).

148 We model 7 faults in the Southern Apennines (Alburni, Irpinia, Irpinia Antithetic, San Gregorio Magno (here  
 149 referred as “San Gregorio”), Val D’Agri, Vallo Di Diano and Volturara faults (Fig. 2a)) and 7 faults in the Central  
 150 Apennines (Fucino-Ovindoli-Pezza (here referred as “Fucino”, also known as San Benedetto dei Marsi-Gioia dei  
 151 Marsi segment by Galadini and Galli (1999)), Liri, Maiella, Monte Marsicano, Scanno, Sulmona (also known as  
 152 Monte Morrone fault by Galli et al. (2015)) and Trasacco faults (Fig. 2b)). All selected faults are active, with  
 153 documented Holocene throw (Faure Walker et al., 2021; Sgambato et al., 2020a; Valentini et al., 2017). In  
 154 preliminary trials, we identified that the inclusion of three other active faults in the Central Apennines (Parasano-

Formatted: English (UK)

Formatted: English (UK)

Deleted: sa

Formatted: English (UK)

Formatted: English (UK)

Formatted: English (UK)

156 ~~Pescina, Tremonti and San Sebastiano faults) led to unrealistically high stress concentrations in the Fucino fault,~~  
157 ~~which caused numerical instability forcing the simulation to stop prematurely. For these computational reasons,~~  
158 ~~we exclude the three active faults from the Central Apennines model. The potential implications of this exclusion~~  
159 ~~are addressed in the Discussion section.~~

160 The trend and average dip of each fault is taken from published sources (Fault2SHA database, Faure Walker et  
161 al. (2021); Mildon et al., (2019); and Sgambato et al., 2020b) (Table 1). For the Central Apennines, we use the  
162 definition of “main fault traces” of Fault2SHA, which represent how faults segments have been interpreted to be  
163 linked at depth, at the scale recommended for input into hazard models (Faure Walker et al., 2021). For the  
164 Southern Apennines, which are not covered by the Fault2SHA database, we utilise fault traces from Sgambato et  
165 al., (2020b). The geometry and extent of some of these fault traces is debated. For instance, in some interpretations  
166 the NW segment of Vallo di Diano fault (also known as Auletta fault or Caggiano fault) is a separate segment  
167 from this fault and continues SE (Galli et al., 2006a) or even joins with Val D’Agri fault as part of the Caggiano-  
168 Montemurro fault system (Bello et al., 2022) (Fig. 1b). Here, we follow the interpretation of Sgambato et al.  
169 (2020b), where the NW segment is part of Vallo di Diano fault based on the field-based evidence of the slip vector  
170 orientations (Papanikolaou and Roberts, 2007).

171 To accommodate QDYN current restriction to a uniform strike for each dip-slip fault, we rectify the fault traces  
172 (Fig. 2). The fault depths are set in most of the cases to 15 km, which is taken as approximately the depth of the  
173 brittle-ductile transition and is consistent with hypocentral depths observed in the region (Chiarabba et al., 2005;  
174 Chiaraluce et al., 2005; Frepoli et al., 2011). We make two exceptions for fault geometry parameters. The Irpinia  
175 Antithetic fault, being relatively short (length < 15 km), is assigned a depth of 8 km to maintain an aspect ratio of  
176 1 (Nicol et al., 1996). This modification has implications for the generation of full ruptures, as addressed in the  
177 Results and Discussion sections. We limited the Alburni fault to a depth of 3 km to prevent numerical instabilities  
178 caused by the intersection with the Vallo di Diano fault. This approximation may lead to an underestimation of  
179 its potential involvement in multi-fault rupture sequences and stress transfer, especially near the Vallo di Diano  
180 fault. However, the Alburni fault is not thought to have ruptured in historical times, but it is considered to have  
181 been active between late Pliocene and late Pleistocene (Gioia et al., 2011; Soliva et al., 2008).

182 We assign a constant loading rate value to each fault, corresponding to the maximum Holocene slip-rate (Figure  
183 2; Cinque et al., 2000; Faure Walker, 2010; Faure Walker et al., 2019, 2021; Galli et al., 2014; Morewood and  
184 Roberts, 2000; Papanikolaou et al., 2005; Roberts and Michetti, 2004; Valentini et al., 2017). Preliminary trials  
185 conducted in this study and from previous work (e.g., Yin, 2022), show that in the implicit LSODA solver used  
186 here (Yin et al., 2023), slip rates below 1 mm/yr can cause velocity values to drop below numerical precision,  
187 especially when neighbouring faults also exhibit low slip rates. We suspect that this is due to the difference  
188 between the minimum and maximum slip rates present in the system, which span many orders of magnitude,  
189 causing precision underflow when jointly solving the system of equations. Therefore, we scale up the loading rate  
190 by a factor of 100 which represents the minimum value required to ensure numerical stability across the full fault  
191 network, while remaining as close as possible to the geologically inferred loading rates. Based on these trials and  
192 on previous studies (Yin, 2022) we find that this scaling has minimal impact on seismicity statistics, once we

**Deleted:** (Yin et al., 2023)

**Deleted:** and to ensure numerical stability arising from fault intersections, we

**Deleted:** in

**Deleted:** from the

**Deleted:** (Parasano-Pescina, Tremonti and San Sebastiano faults)...

**Deleted:** Tremonti and Parasano-Pescina faults are relatively short (<10 km), while the San Sebastiano fault exhibits a maximum Holocene slip rate of 0.37 mm/yr, much slower than the other faults in the network, which range from 1.08 to 1.99 mm/yr (Papanikolaou et al., 2005; Roberts and Michetti, 2004). These three faults are likely to have a minor contribution to the regional seismic hazard and therefore can be excluded from our models.

**Deleted:** used here

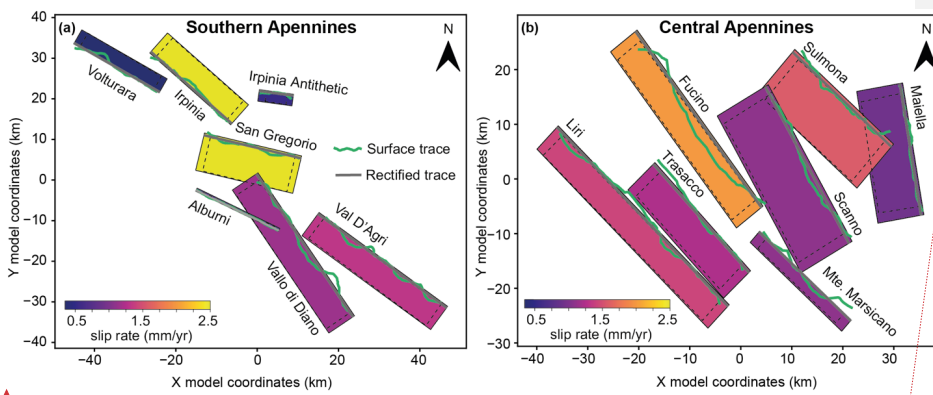
**Deleted:** to keep numerical stability,

**Deleted:** .

211 correct simulations outputs (such as recurrence times) for this upscaling factor (see Appendix B). All time scales  
 212 reported hereafter account for this correction factor.

213 The set up does not contain further complexities such as variable fault geometry, heterogeneous slip-rate  
 214 distribution along the fault strike, and or complex heterogeneous distribution of frictional properties. Although  
 215 these elements may generate heterogeneous stress concentrations that might act as barriers to rupture propagation  
 216 or as regions of earthquake nucleation (Delogkos et al., 2023; Hillers et al., 2007; Luo and Ampuero, 2018; Mildon  
 217 et al., 2019; Rodriguez Piceda et al., 2025a), we chose to omit these complexities to primarily focus on the impact  
 218 of fault network geometry and fault stress interactions on rupture dynamics.

Deleted: .



Formatted: English (UK)

220 **Fig. 2: Map view of the model geometry for the (a) Southern Apennines and (b) Central Apennines fault**  
 221 **network. Fault planes are colour-coded according to their Holocene slip rate. Black dashed lines show the**  
 222 **velocity-weakening asperities. Surface fault traces (green) derived from (Faure Walker et al., 2021; Mildon**  
 223 **et al., 2019; Sgambato et al., 2020b) and rectified traces (grey) used in the model are also shown.**

225 **Table 1: Geometry and long-term slip rate of modelled fault sources in the Southern and Central Apennines.**  
 226 References for slip rate: [1] (Valentini et al., 2017) [2] (Faure Walker, 2010) [3] (Galli et al., 2014) [4] (Cinque  
 227 et al., 2000) [5] Fault2SHA database (Faure Walker et al., 2021) [6] (Morewood and Roberts, 2000) [7] (Roberts  
 228 and Michetti, 2004) [8] (Faure Walker et al., 2019a) [9] (Papanikolaou et al., 2005)

Modelled region	Fault	Map trace length (km)	Average fault dip (deg)	Maximum long-term slip rate (mm/yr)
	Alburni fault	23	74	0.7 [1] [2]

Southern Apennines	Irpinia fault	27	66	2.5 [1] [3]
	Irpinia Antithetic fault	8.5	70	0.53 [1] [2]
	San Gregorio fault	24	58	2.5 [1] [3]
	Val D'Agri fault	39	64	1.3 [1] [2]
	Vallo Di Diano fault	42	63	1.15 [1] [4]
	Volturara fault	24	75	0.35 [1] [2]
Central Apennines	Fucino fault	40	66	1.99 [5] [6]
	Liri fault	47	68	1.41 [5] [7]
	Maiella fault	24	58	0.92 [5] [7]
	Monte Marsicano fault	24	7	1.08 [5] [7]
	Scanno fault	33	52	1.08 [5] [8]
	Sulmona fault	26	54	1.57 [5] [9]
	Trasacco fault	27	64	1.22 [5] [7]

230

231 The simulations run for 11 kyrs to ensure a sufficient number of seismic events for statistical analysis, with the  
232 first 500 years discarded as the spin-up phase. To compute the duration of a seismic event, we consider that it

233 starts when one fault element has a slip rate larger than 0.1 m/s and stops when the slip rate of all the elements  
234 slip drops below 0.01 m/s.

235 We additionally simulate SEAS on each individual isolated fault included in the Southern and Central Apennines  
236 networks to determine their reference behaviour in the absence of stress interactions with other faults. These  
237 simulations use the same parametrization as the full fault network simulations described above.

### 238 3.2 Fault network and seismic cycle characteristics

239 To quantify the effect of across-strike faults, we compute an across-strike interaction index ( $AI$ ) for each fault  $i$   
240 as:

$$241 \quad AI_i = \sum_{j \neq i} \frac{1}{s_{ij}} \quad (1)$$

242 where  $j$  are the indices of other across-strike faults,  $s_{ij}$  is the across-strike separation between fault  $i$  and fault  $j$   
243 (see Appendix C for a detailed definition of the separation between faults). The inverse weighting  $\frac{1}{s_{ij}}$  ensures that  
244 faults that are closer contribute more to the index than those farther away. Faults with a larger number of across-  
245 strike interactions have a higher across-strike interaction index. We focus on across-strike density since previous  
246 work (Rodríguez Picada et al., 2025a) showed that across-strike interactions dominate over along-strike  
247 interactions at comparable distances.

Deleted: (Rodríguez Picada et al., 2025)

248 To characterise the complexity of seismic cycles, we compute three metrics: the coefficient of variation of  
249 recurrence times of individual faults ( $CV_{Tr}$ ), the normalised number of partial ruptures ( $N_p'$ ) and the coefficient  
250 of variation of rupture lengths ( $CV_{RL}'$ ).

251  $CV_{Tr}$  is calculated as:

$$252 \quad CV_{Tr} = \frac{std(T_r)}{mean(T_r)} \quad (2)$$

253 where  $T_r$  is the distribution of time intervals between consecutive events on the same fault.  $CV_{Tr} = 0$  indicates  
254 strictly periodic seismic cycles;  $0 < CV_{Tr} < 0.5$ , strongly periodic;  $0.5 \leq CV_{Tr} \leq 1$ , weakly periodic;  $CV_{Tr} = 1$  indicates  
255 that event timing is random and independent of other events; and  $CV_{Tr} > 1$  implies event clustering (Boschi et al.,  
256 1995).

257  $N_p'$  is calculated as:

$$258 \quad N_p' = \frac{N_p}{N(W_s/L_{\infty})} \quad (3)$$

259 where  $N_p$  is the number of partial ruptures,  $N$  the total number of events for each fault,  $W_s$  the seismogenic width  
260 and  $L_{\infty}$  the nucleation length (Eq. A5) introduced by Rubin and Ampuero (2005).

Deleted: Rubin and Ampuero (2005)

Deleted: (

Deleted: ,

261  $CV_{RL}'$  is calculated as:

266 
$$CV_{RL}' = \frac{(std(RL)/mean(RL))}{(W_s/L_\infty)} \quad (4)$$

267 where  $RL$  is the distribution of rupture lengths.

268 Both  $N_p'$  and  $CV_{RL}'$  are normalised by  $W_s/L_\infty$  to account for fault-to-fault differences in seismogenic width  $W_s$   
 269 and the nucleation length  $L_\infty$ , enabling comparison of partial ruptures and rupture length variability (Cattania,  
 270 2019; Barbot, 2019). Overall, faults with larger  $CV_{T_p}$ ,  $N_p'$ ,  $CV_{RL}'$  have seismic cycles characterised by less periodic  
 271 recurrence, more frequent partial ruptures and a wider range of rupture sizes.

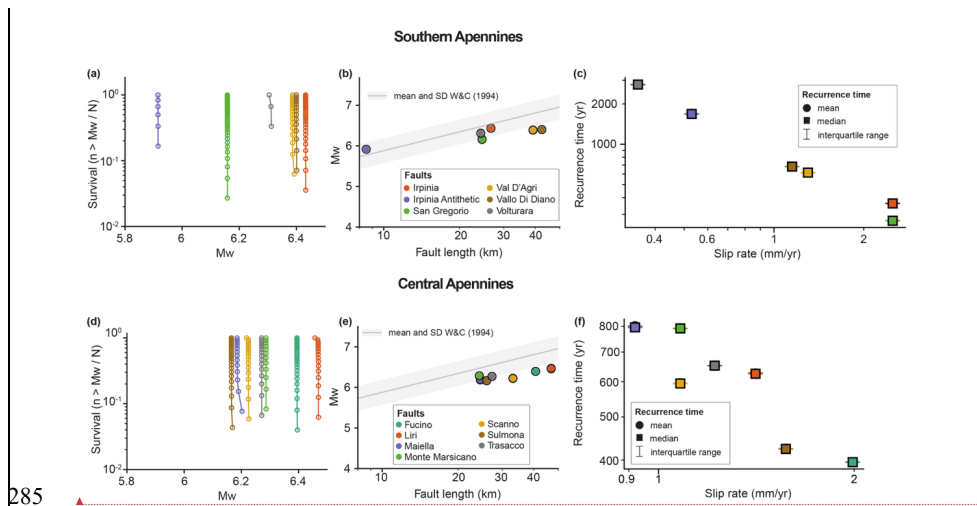
272

273 **4 Results**

274 **4.1 Seismic cycles on isolated faults**

275 In all single-fault simulations, faults rupture with a characteristic magnitude  $M_w$  (Fig. 3a,d), which is linearly  
 276 related to the logarithm of fault length (Fig. 3b,e). In the Southern Apennines,  $M_w$  on individual faults ranges  
 277 from 5.9 for the Irpinia Antithetic fault to 6.4 for the Irpinia and Vallo di Diano faults (Fig. 3a). In the Central  
 278 Apennines,  $M_w$  values range from 6.2 on the Sulmona fault to 6.5 on the Liri fault (Fig. 3d). Notably, most  
 279 earthquakes in both fault networks have magnitudes smaller than those predicted by empirical relationships of  
 280 subsurface rupture length vs. magnitude (Fig. 3b,e; Wells and Coppersmith, 1994).

281 The resulting seismic cycles are periodic, with recurrence intervals inversely correlated to the prescribed long-  
 282 term slip rate (Fig. 3c,f). Mean recurrence times range from 300 years in San Gregorio fault to ~1700 years in  
 283 Volturara fault in the Southern Apennines (Fig. 3c); and from 400 years in Fucino fault to 800 years in Maiella  
 284 fault in the Central Apennines (Fig. 3f).



285

Formatted: English (UK)

286 **Figure 3: Earthquake cycle simulations of isolated faults in the (a-c) Southern and (d-f) Central Apennines.**  
 287 **(a, d) Magnitude-frequency distributions of earthquakes on each fault (shown as survival functions:**  
 288 **number of events with a Mw larger than a given value, normalised by the total number of events). Their**  
 289 **near vertical appearance indicates all isolated faults in this model have characteristic-earthquake**  
 290 **behaviour, with very narrow range of Mw. (b, e) Comparison between modelled seismic events and mean**  
 291 **and standard deviation of empirical relationships of subsurface rupture length vs. Mw (Wells and**  
 292 **Coppersmith, 1994); (c, f) Mean, median and interquartile range of earthquake recurrence times vs. long-**  
 293 **term tectonic slip rate of individual faults. Note how the mean and median are equal, and the interquartile**  
 294 **range is below the marker size for all faults across both regions.**

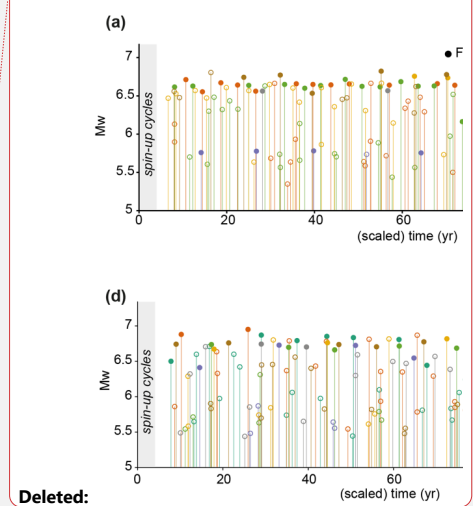
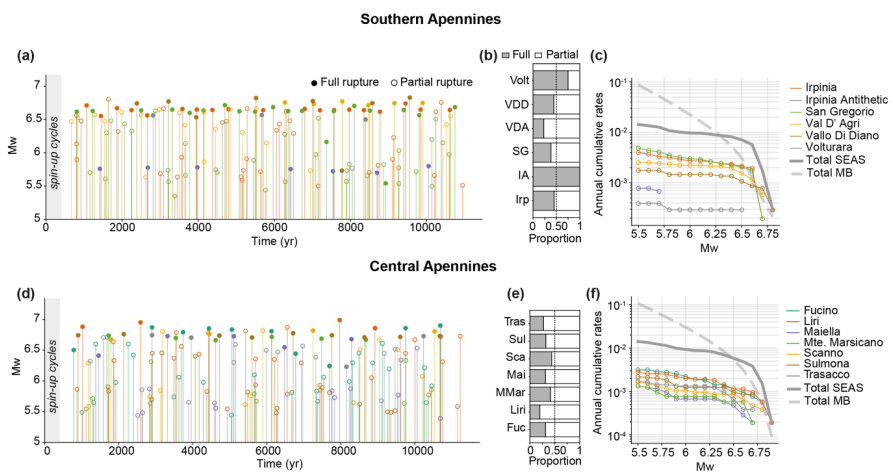
295 **4.2. Seismic cycles on fault networks**

296 We generated two synthetic seismic catalogues for the interacting fault networks, containing 150 events in the  
 297 Southern Apennines and 154 events in Central Apennines (Fig. 4a,d). The magnitude range produced by faults  
 298 within the networks is broader than that of isolated faults: from Mw 5.3 to 6.8 in the Southern Apennines (Fig.  
 299 4c) and from Mw 5.3 to 7 in the Central Apennines (Fig. 4f), broadly matching observed earthquake magnitudes.  
 300 In our Southern Apennines model, the Alburni fault does not produce any earthquakes. This is likely due to its  
 301 shallow seismogenic zone (down to a depth of 2.65 km). Unlike the isolated fault models, not all ruptures extended  
 302 for the whole length of the faults, with some ruptures terminating as partial ruptures. Most faults generate both  
 303 full and partial ruptures, with a larger proportion of partial ruptures (Fig. 4b,e). Due to the generation of full  
 304 and partial ruptures, the magnitude-frequency distributions show a truncated Gutenberg-Richter distribution (Stirling  
 305 et al., 1996). The largest magnitude events are limited by the length of the longest fault, in our case, the Vallo di  
 306 Diano fault in Southern Apennines (Fig. 4c) and the Liri fault in Central Apennines (Fig. 4f). The Irpinia Antithetic  
 307 fault is the only fault to consistently generate full ruptures with a characteristic Mw of 5.8. This is likely due to  
 308 its small fault dimensions (8 km in length and depth), which limits its potential for partial ruptures in the model  
 309 (Barbot, 2019; Cattania, 2019; Cattania and Segall, 2019) (Fig 4b,c).

Deleted: s

Deleted: c

Deleted: f



Deleted:  
Formatted: English (UK)

310

315 **Figure 4: Earthquake statistics from the model results for the Southern (a-c) and Central (d-f) Apennines**  
 316 **fault networks. Time distribution of simulated full- and partial-rupture events with stems and markers**  
 317 **colour-coded by fault in the (a) Southern Apennines and (d) Central Apennines. Earthquakes in the first 5**  
 318 **yrs correspond to spin-up phases, thus are not included in the analysis. (b, e) proportion of full and partial**  
 319 **ruptures relative to the total number of events per fault in the (b) Southern Apennines and (e) Central**  
 320 **Apennines. (c, f) Magnitude–frequency distributions of seismic events expressed as annual cumulative rates**  
 321 **(number of annual occurrences with Mw greater than a given value) for individual faults in the (c) Southern**  
 322 **Apennines and (f) Central Apennines. Annual cumulative rates for the entire fault network derived from**  
 323 **the SEAS models, together with estimates obtained using the moment-budget method (MB; Appendix H),**  
 324 **are also shown. Colour legend for each fault is shown in panels (c) and (f).**

325

326 To highlight the rupture styles observed in our simulation, Figure 5 shows a subset of events that occur in the  
 327 Central Apennines between two full ruptures, one on the Liri fault and one on the Maiella fault. While a full  
 328 rupture occurs on one fault, the remaining faults stay locked (Fig. 5a). The full rupture affects both the locked and  
 329 surrounding creeping segment of the fault (Fig. 5a), and it is followed by partial ruptures in the remaining faults  
 330 (Fig. 5b-h). Some of these partial ruptures occur consecutively on the same fault (e.g. Fucino fault, Fig. 5g-h),  
 331 with some separated by hours (e.g. two events on the Vallo di Diano fault at 5450 yr and two events on the Monte  
 332 Marsicano fault at 8360 yr, not shown in Fig. 5, Videos S2, S3; (Rodriguez Piceda et al., 2026)). Subsequent  
 333 events in this type of sequence commonly rupture the fault segments that were not involved in the prior earthquake.  
 334 Simulated full and partial ruptures nucleate typically at the base of the locked seismogenic zone (Videos S2-S3,  
 335 (Rodriguez Piceda et al., 2026)). Overall, while full-rupture events homogenise the slip rate field in locked fault  
 336 patches (Fig. 5b), partial ruptures introduce a heterogeneous slip rate field in these patches (Fig. 5f), a direct  
 337 consequence of the stress concentration left behind by the arrested partial ruptures. The heterogeneous slip rate  
 338 then influences the nucleation and propagation of subsequent events (Video S2; (Rodriguez Piceda et al., 2026)),  
 339 acting either as nucleation sites or barriers where ruptures terminate. In addition to the observed earthquakes,  
 340 aseismic slip in the form of slow slip events sometimes occurs simultaneously with seismic events on other faults  
 341 (Fig. 5c, Video S2, (Rodriguez Piceda et al., 2026)). The occurrence of full and partial ruptures, as well as slow-  
 342 slip events, shows the more diverse slip behaviour of faults within a network compared to the isolated fault models.

**Deleted:** Given the use of a scaled slip rate, note that the simulated time (~110 yrs in both catalogues) is approximately equivalent to 11,000 yrs.

**Deleted:** (c, f) Magnitude-frequency distributions of seismic events shown as survival function (number of events with a Mw larger than a given value normalised by total number of events) for each fault in (c) Southern Apennines and (f) Central Apennines.

**Deleted:** tens of seconds

**Deleted:** .

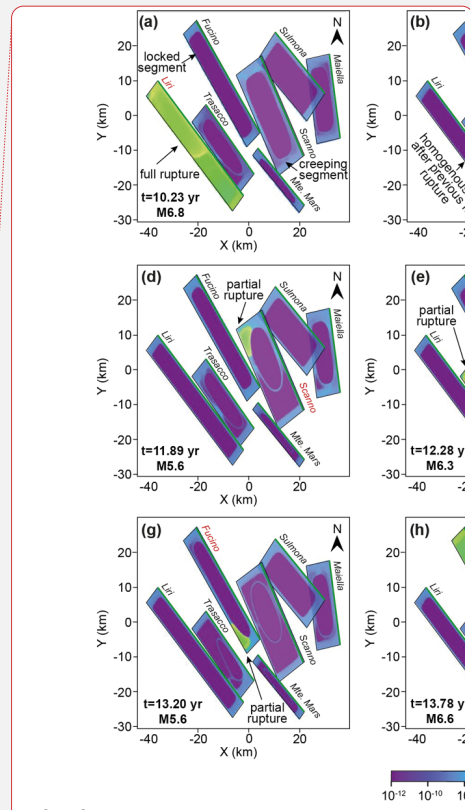
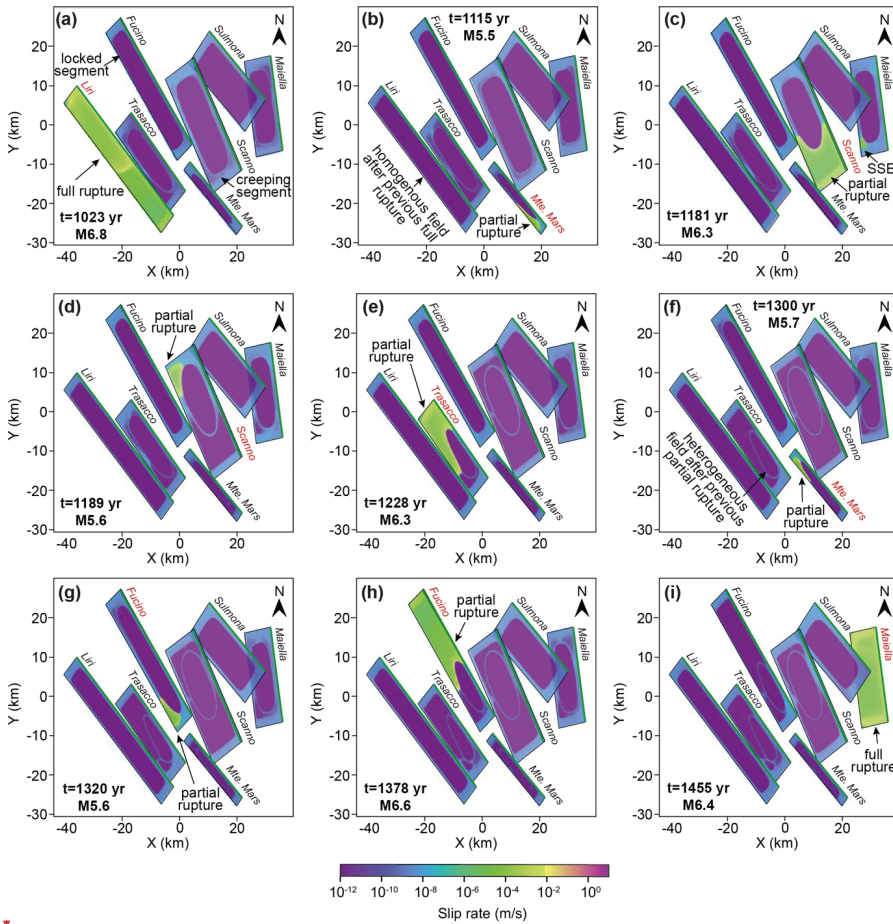
**Deleted:** .

**Deleted:** ;

**Deleted:** Rodriguez Piceda et al., 2025c

**Deleted:** Rodriguez Piceda et al., 2025c

**Deleted:** (Rodriguez Piceda et al., 2025c



Deleted:

Formatted: English (UK)

358

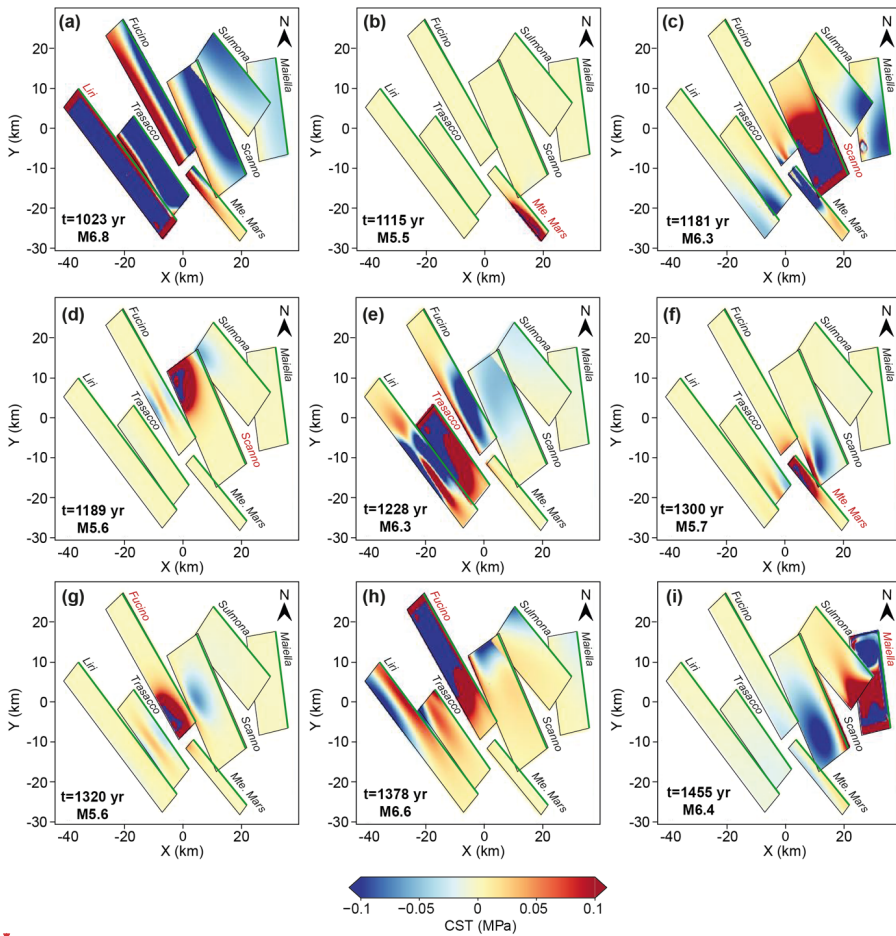
359 **Figure 5: Map view of slip-rate snapshots showing the final timestep of the coseismic phase for each event**  
 360 **in a subset of modelled ruptures in the Central Apennines including full ruptures, partial ruptures and**  
 361 **slow slip events (SSE). Monte Marsicano fault is abbreviated as Mte. Mars.**

362 To illustrate the stress changes introduced by each seismic event we computed the coseismic Coulomb stress  
 363 transfer (CST) for each seismic event as (King et al., 1994):

$$364 \Delta C = \Delta \tau - \mu(\theta, V) \Delta \sigma \quad (5)$$

365 where  $\Delta \tau$  is the shear stress-change,  $\Delta \sigma$  is the normal stress change before and after the earthquake and  $\mu(\theta, V)$   
 366 the rate-and-state friction coefficient at the receiver fault location. Figure 6 shows the CST for the same subset of  
 367 modelled ruptures as in Fig. 5, and the CST evolution from all events in both fault network models are shown in  
 368 Figs. S5 and S6. Most full and partial ruptures introduce a heterogeneous stress change on nearby faults, due to

370 the range of fault strike and partial overlaps between faults in the network (Fig. 6). In the rare cases where faults  
 371 are almost parallel and with a near 100% overlapping area, a full-rupture event on one fault introduces a  
 372 homogenous stress change. This can be observed for the Liri and Trasacco faults, where a full-rupture event on  
 373 Liri fault negatively loads Trasacco fault (Fig. 6a).

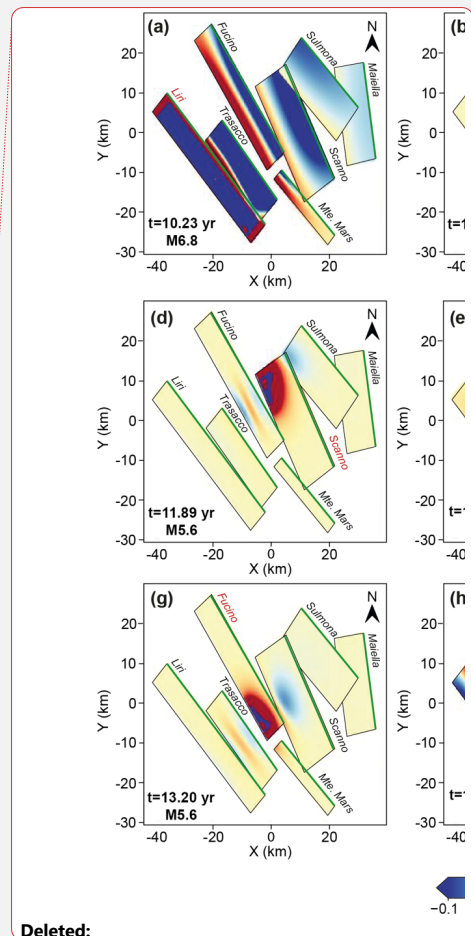


374

375 **Figure 6: Coseismic Coulomb Stress Transfer (CST) for a subset of modelled earthquakes in the Central**  
 376 **Apennines shown in Fig. 5, with fault planes projected to a horizontal surface.**

377

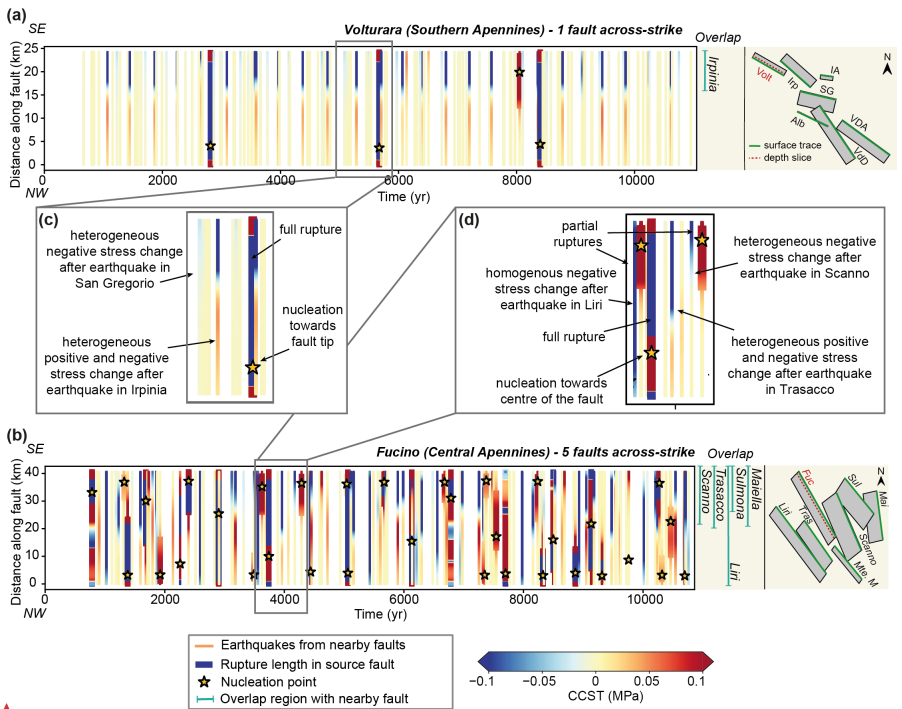
378 Figure 7a-b shows the evolution of CST and nucleation point of each event along a depth slice near the top of the  
 379 velocity-weakening asperities (~1700 m) of the Volturara and Fucino faults, compared to the extent of overlap  
 380 with adjacent faults in the fault network (Figures S7 and S8 show the same but for the remaining faults). Faults



Deleted:  
 Formatted: English (UK)

382 such as Volturara, which have few nearby, partially overlapping, across-strike faults, tend to show coseismic stress  
 383 changes that remains broadly similar through successive earthquake cycles. Seismicity comprises mainly full  
 384 ruptures that nucleate near fault tips (Fig. 7a, c). These nucleation locations correspond to regions of elevated  
 385 stressing rates produced by the backslip loading method, which remain highest near fault tips despite the inclusion  
 386 of velocity-strengthening buffer regions (Appendix A).

387 Conversely, faults with multiple neighbouring across-strike faults, such as Fucino fault (Fig. 7b, d), show a more  
 388 spatially heterogeneous stress evolution and complex earthquake cycles consisting of full and partial ruptures.  
 389 Additionally, the nucleation of full and partial ruptures is not necessarily confined to fault tips. Instead, partial  
 390 ruptures that are either isolated or the first in a sequence often occur in areas where faults overlap. Therefore, the  
 391 number and arrangement of across-strike faults, and the heterogeneous coseismic stress changes they induce, have  
 392 a strong control on the earthquake cycle of individual faults.



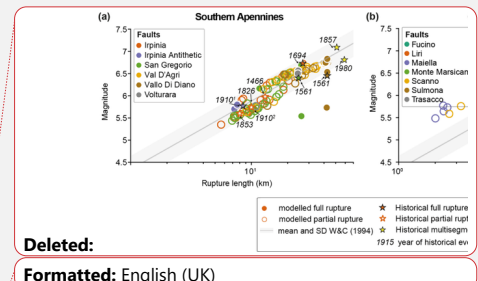
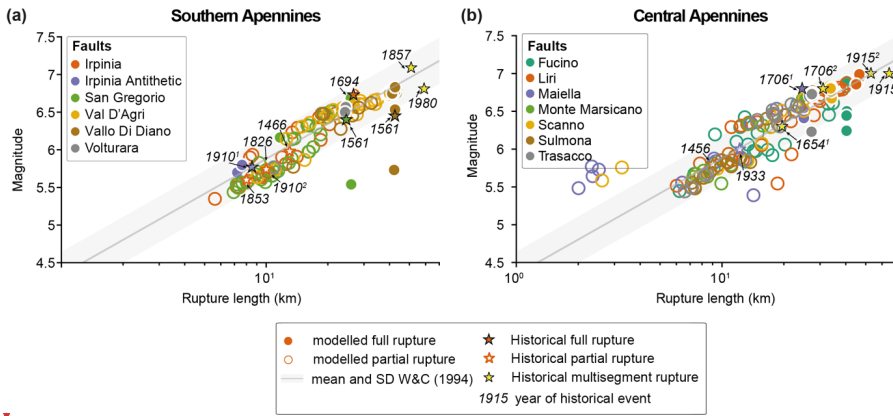
393  
 394 **Figure 7: (a) Coseismic Coulomb stress transfer (CST) on the Volturara fault, which has 1 across-strike**  
 395 **fault that overlaps; (b) CST on the Fucino fault, which has 5 neighbouring across-strike faults that overlap.**  
 396 **Coloured backgrounds show the stress changes following each event along a depth slice close to the top of**  
 397 **the velocity weakening asperity (location example shown in right panels of Fig. 7a,b). Coseismic CST due**  
 398 **to ruptures on the fault are indicated by the thick vertical slices that coincide with a star (nucleation point**  
 399 **on the fault); thin vertical slices without corresponding star represent the coseismic CST due to ruptures**

- Deleted:
- Deleted: with
- Deleted: nearby
- Deleted: , such as Volturara,
- Deleted: heterogeneous coseismic stress changes from neighbouring faults and simple earthquake cycles
- Deleted:
- Deleted: ing
- Moved (insertion) [2]
- Deleted: .
- Moved up [2]: (Fig. 7a, c).
- Deleted: (Fig. 7a, c).
- Deleted: non-coplanar

Formatted: English (UK)

412 on neighbouring faults. On the right side of panels (a) and (b) we indicate the fault segments that are  
 413 overlapping with neighbouring faults (taken as the maximum length measured along-strike from the NW  
 414 fault tip, see Fig. D2, Appendix D), including an inset with map view of fault surfaces. (c) and (d) are zoom-  
 415 ins highlighting contrasting behaviours between the faults. The Volturara fault shows spatially  
 416 homogeneous stress changes and simple seismic cycles, with full ruptures and nucleation near fault tips.  
 417 The Fucino fault exhibits spatially complex coseismic CST patterns, partial ruptures, and nucleation that  
 418 is more distributed across the fault. Faults with limited across-strike interaction tend to show simpler  
 419 rupture behaviour, while those with multiple across-strike interactions show a more heterogeneous stress  
 420 evolution and complex earthquake cycle.

421 We compared the magnitudes and rupture lengths of the modelled events with historical seismicity (Table B1,  
 422 Appendix B) and empirical relationships between magnitude and subsurface rupture length (Wells and  
 423 Coppersmith, 1994); Fig. 8a-b). Our models are able to reproduce the magnitude and rupture length of the  
 424 historical single-fault events, including the two proposed scenarios for the 1910 earthquakes in Southern  
 425 Apennines (Galli and Peronace, 2014). However, we are unable to reproduce multi-fault events as recorded in the  
 426 historical seismicity catalogue (e.g. the 1857 and the 1980 seismic sequences in the Southern Apennines; one of  
 427 the proposed scenarios for the 1706 sequence and the 1915 sequence in the Central Apennines; Table B1,  
 428 Appendix B). Compared to the empirical relationships of magnitude vs. subsurface length, most of our modelled  
 429 events (99% in Southern Apennines and 92% in Central Apennines) fall within the range marked by the mean and  
 430 standard deviation of Wells & Coppersmith (1994).



Deleted:  
 Formatted: English (UK)

431  
 432 **Figure 8: Comparison between modelled seismic events, historical ruptures and empirical relationships of**  
 433 **subsurface rupture length vs. Magnitude (Wells and Coppersmith; 1994) for (a) Southern Apennines and**  
 434 **(b) Central Apennines. Magnitude refers to Mw for SEAS simulations and empirical scaling relationships;**  
 435 **magnitudes of historical earthquakes are defined in Table B1 (Appendix B). Modelled and historical single-**  
 436 **fault events are colour-coded according to the source fault. Superindices on dates of historical events refer**  
 437 **to alternative scenarios. 1910<sup>1</sup>: scenario with rupture of entire Irpinia antithetic (Galli and Peronace, 2014);**  
 438 **1910<sup>2</sup>: scenario with 10-km rupture of Irpinia fault (Galli and Peronace, 2014); 1654<sup>1</sup>: scenario with 13-km**

Deleted: w

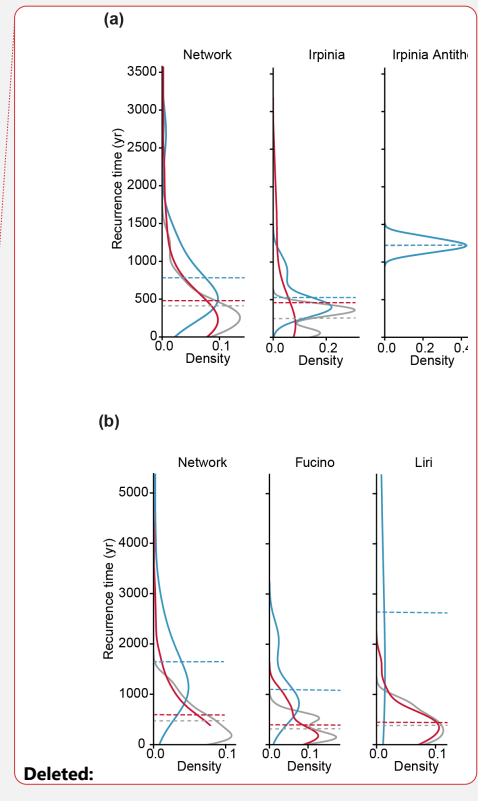
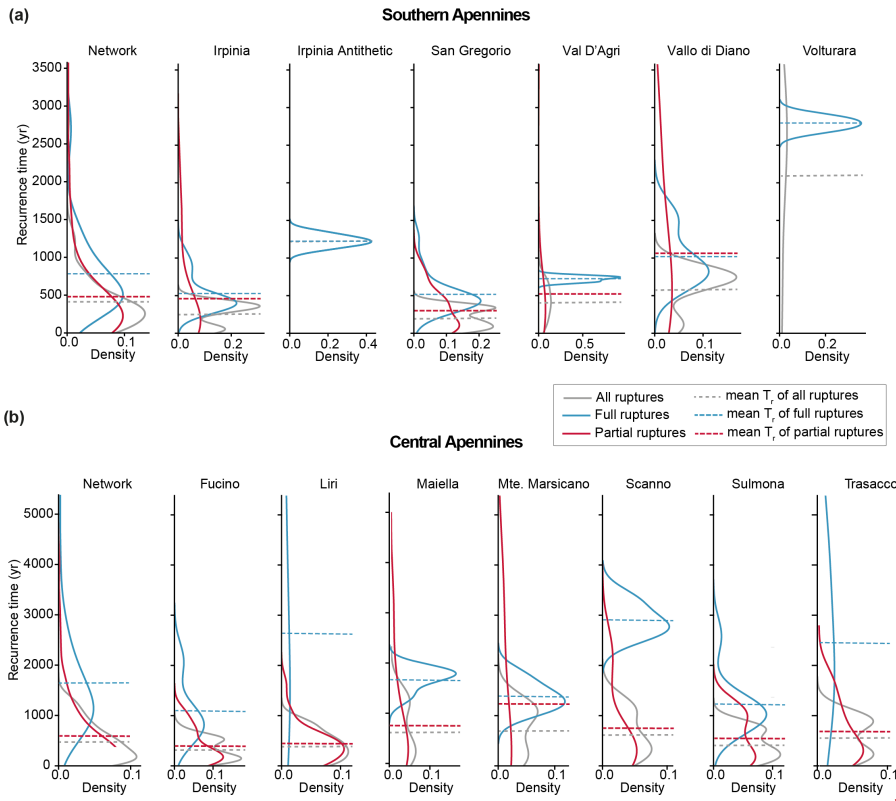
441 rupture of Southern section of Liri and entire Fibreno faults (outside of study area; (Guidoboni *et al.* 2019);  
442 1706<sup>1</sup>: scenario with rupture of entire Maiella fault (Guidoboni *et al.*, 2019); 1706<sup>2</sup>: scenario with rupture  
443 of entire Maiella and Palena faults (outside of study area; (Guidoboni *et al.*, 2019); 1915<sup>1</sup> scenario with  
444 rupture of entire Fucino, Parasano and San Sebastiano faults (Michetti *et al.*, 1996); 1915<sup>2</sup> scenario with  
445 rupture of entire Fucino, Luco and Trasacco faults (Michetti *et al.*, 1996) (see Table B1, Appendix B).

446

447 Recurrence times vary between the two modelled regions, and depend on whether the full catalogue is considered,  
448 or whether it is split between full and partial ruptures. Full catalogue recurrence times for the system and for  
449 individual faults are positively skewed, with some faults showing bi-modal distributions (Fig. 9). When the  
450 Southern and Central Apennines are compared, greater variability is observed in the mean recurrence times of the  
451 Southern Apennines, which range from 250 (San Gregorio fault) to 2100 (Vulturara fault) years in the Southern  
452 Apennines compared to 300 (Fucino fault) and 700 (Monte Marsicano fault) years in the Central Apennines (Fig.  
453 9).

454 Where full and partial rupture catalogues are compared, partial ruptures tend to have shorter recurrence times than  
455 full ruptures (Fig 9a-b). Across both regions, recurrence time distributions of partial ruptures in individual faults  
456 and the system are positively skewed, spanning a wide range, from ~~hours~~ to years. In contrast, the recurrence time  
457 distributions of full ruptures are narrower, typically following a bimodal or normal distribution (Fig 9).

Deleted: seconds



459

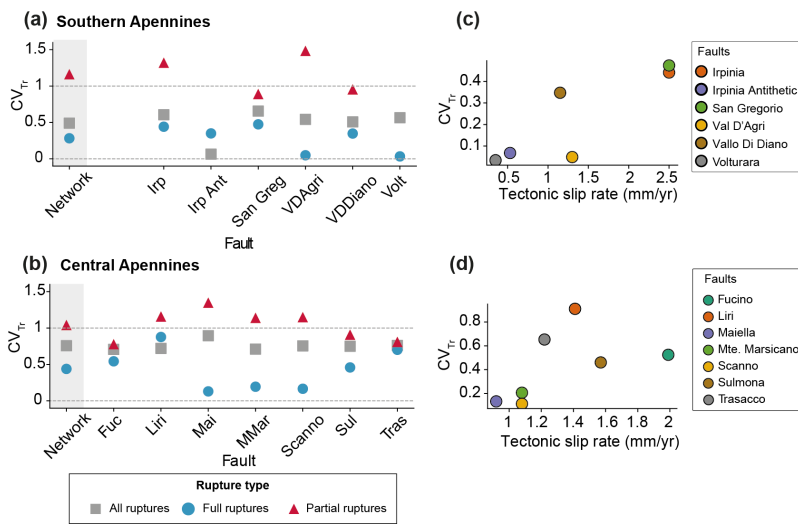
460 **Figure 9: Variation of recurrence time ( $T_r$ ) for the (a) Southern and (b) Central Apennines, shown as kernel**  
 461 **density plots (KDE) and mean recurrence time, for the entire fault network and for individual faults**  
 462 **considering the 'All-ruptures', 'Full-ruptures' and 'Partial-ruptures' catalogues. Volturara fault produced**  
 463 **only 1 partial rupture, thus no KDE for its partial-rupture catalogue could be computed. As this single**  
 464 **partial rupture is included in the 'All-ruptures' catalog but absent from the 'Full-rupture' catalog, the two**  
 465 **distributions are different. Note how the density scale varies by fault, and that partial ruptures typically**  
 466 **display a greater range in recurrence time than full ruptures.**

467 The catalogue periodicity is assessed through the coefficient of variation of recurrence time  $CV_{T_r}$ . For the all-  
 468 rupture catalogues, both regions display weakly periodic behaviour ( $CV_{T_r}=0.5-1$ , Fig. 10a-b). The exception is the  
 469 Irpinia Antithetic fault, which maintains a more periodic recurrence (Fig. 10a). Overall, the Central Apennines  
 470 exhibits less periodic seismic cycles ( $CV_{T_r}=0.8$ , Fig. 10b) compared to the Southern Apennines ( $CV_{T_r}=0.5$ , Fig.  
 471 10a).

472 Periodicity differs between full and partial ruptures as well as between regions. Faults generate full rupture events  
 473 with varying degrees of periodicity. In the Southern Apennines (Fig. 10a), all faults show strongly periodic full-  
 474 rupture cycles ( $CV_{T_r}<0.5$ ). In the Central Apennines (Fig. 10b), the behaviour is more variable: the Maiella,

476 Monte Marsicano and Scanno faults show strongly periodic full-rupture cycles whereas the Trasacco, Liri,  
 477 Sulmona and Fucino faults are weakly periodic ( $0.5 \leq CV_{Tr} < 1$ ). Partial ruptures in both networks show less periodic  
 478 behaviour than full ruptures (Fig. 10a-b). Their recurrence ranges from weakly periodic ( $0.5 \leq CV_{Tr} < 1$ ; e.g., San  
 479 Gregorio, Fucino, Sulmona and Trasacco faults) to random ( $CV_{Tr}=1$ , e.g., Vallo di Diano fault) or clustered  
 480 ( $1 < CV_{Tr} < 1.5$ , e.g., Irpinia, Val D'Agri, Liri, Maiella, Monte Marsicano and Scanno faults).  $CV_{Tr}$  of full-rupture  
 481 events tends to increase with increasing long-term slip rate (Fig. 10c-d).

482



483

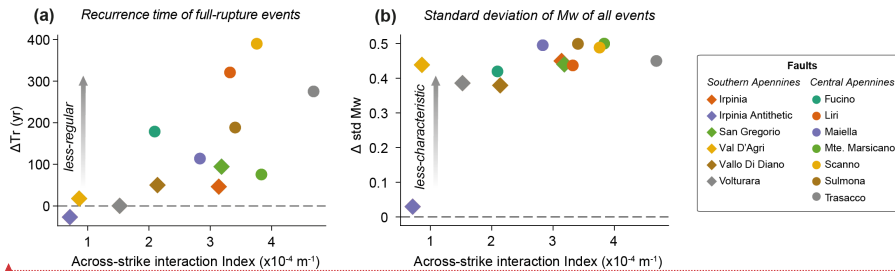
484 **Figure 10: (a-b) Coefficient of variation of recurrence times  $CV_{Tr}$  of seismic events (all events, full ruptures**  
 485 **and partial ruptures) for individual faults and entire fault network in the (a) Southern Apennines and (b)**  
 486 **Central Apennines. Horizontal dashed lines mark the  $CV_{Tr}$  values of perfectly periodic ( $CV_{Tr}=0$ ) and lower**  
 487 **limit of random ( $CV_{Tr}=1$ ) seismic cycles. (c-d) Long-term slip rate vs.  $CV_{Tr}$  of all events for the (c) Southern**  
 488 **Apennines and the (d) Central Apennines. Seismic cycles of full-rupture events are either strongly or**  
 489 **weakly periodic, while cycles of partial ruptures are weakly periodic, random or clustered. The fault**  
 490 **network in the Central Apennines has less periodic seismic cycles than in the Southern Apennines.**

491 **4.3 Relationships between seismic cycle characteristics and fault network geometry**

492 In the Southern Apennines, where the fault network has fewer across-strike faults and larger distances between  
 493 them, the across-strike interaction index (AI) is less than in the Central Apennines, which has multiple closely-  
 494 spaced across-strike faults, resulting in a higher AI due to both fault number and proximity. Fault interactions via  
 495 stress transfer affect recurrence intervals and magnitudes of full-rupture events, compared to the isolated fault  
 496 case (Fig. 11). Most faults produce full ruptures with longer recurrence times and larger magnitudes compared to

497 the reference cycles on isolated fault (Fig. 11). These differences become more pronounced with an increase in  
 498 the number of nearby cross-strike faults in the Central Apennines, as opposed to the Southern Apennines.

499



500

501 **Figure 11: Comparison of earthquake cycles between single-fault simulations and fault-network**  
 502 **simulations in terms of event (a) recurrence time ( $Tr$ ) of full-rupture events ( $\Delta Tr = \text{mean } Tr_{\text{network}} -$**   
 503  **$\text{mean } Tr_{\text{single}}/\text{mean } Tr_{\text{single}}$ ) and (b) standard deviation of magnitude of full-rupture events**  
 504  **$\Delta std Mw = std Mw_{\text{network}} - std Mw_{\text{single}}$ ) as a function of the across-strike interaction index (eq. 1).**  
 505  **$\Delta Tr=0$  indicates regular recurrence, while positive (negative) values correspond to longer (shorter)**  
 506 **recurrence times in the fault-network simulations relative to the single-fault simulations.  $\Delta std Mw=0$**   
 507 **indicates characteristic magnitude distribution, while increasingly positive values indicate broader**  
 508 **magnitude-frequency distributions in the fault-network simulations. Faults with multiple faults across-**  
 509 **strike (larger  $AI$ ) show larger differences in recurrence time and standard deviations of magnitude**  
 510 **compared to single-fault simulations, indicating a greater deviation from their characteristic periodic**  
 511 **behaviour.**

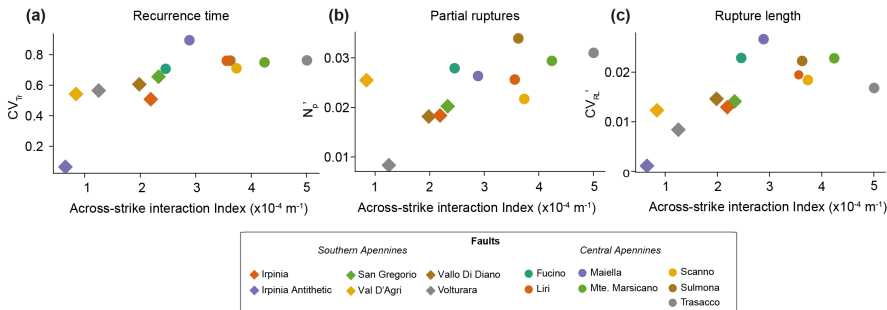
512 Differences in earthquake cycle properties between the Southern and Central Apennines are influenced by fault  
 513 network geometry (Fig. 12). When considering both networks together, we observe consistent positive  
 514 correlations between the across-strike interaction index  $AI$  and the three metrics of seismic complexity ( $CV_{Tr}$ ,  $N_p'$ ,  
 515 and  $CV_{RL}'$ ) with mean Spearman values ranging from 0.46 to 0.84 (Table F1, Appendix F). When analysed  
 516 separately, the Southern Apennines show strong correlations for  $CV_{Tr}$  and  $CV_{RL}'$  at some depths (Table F1), but no  
 517 consistent trend for  $N_p'$ . In contrast the Central Apennines show weak or no correlations for all metrics (Table  
 518 F1). This suggest that the geometric effects become clearer when sampling a broader range of network  
 519 configurations across both regions.

520

Formatted: English (UK)

Deleted: G

Deleted: Southern



523

524 **Figure 12: Relationships between fault network geometry, described by the across-strike interaction index**  
 525 **(AI), and (a) coefficient of variation of recurrence times ( $CV_{Tr}$ ), (b) number of partial ruptures ( $N_p'$ ) and**  
 526 **coefficient of variation of rupture lengths ( $CV_{RL}'$ ) for faults in the Southern and Central Apennines. AI is**  
 527 **calculated at a depth of 7.5 km, approximately the middle fault depth. Plots corresponding to depths of 0**  
 528 **km and 15 km are shown in Fig. F1 (Appendix F).**

529

## 530 5 Discussion

### 531 5.1 Comparison between simulated and natural seismic cycles in Italy

532 Italy's exceptional historical and paleoseismic record (D'Addezio et al., 1991; Galadini and Galli, 1996, 1999;  
 533 Galli et al., 2006, 2008, 2016, 2014; Galli and Peronace, 2014; Pace et al., 2020; Pantosti et al., 1993) provides a  
 534 valuable basis for evaluating our models. Our simulations are, to our knowledge, the first 3D continuum  
 535 earthquake cycle models to combine rate-and-state friction with fault interactions across more than three faults,  
 536 resolving nucleation and rupture self-consistently.

537 To compare with natural data, we focused on  $M \geq 6.5$  events and recurrence intervals from paleoseismic trenching  
 538 (Table B2; Pace et al., 2016). After scaling due the high slip rates used in our models, natural recurrence intervals  
 539 are 1.3-9.4x longer than simulated ones, consistent with our use of maximum along-strike long-term slip rates,  
 540 which likely overestimate loading and shorten cycles. We expect that incorporating realistic tapered profiles  
 541 would bring simulated intervals closer to observations (Delogkos et al., 2023; Faure Walker et al., 2019).

542 Paleoseismic recurrence times show greater variability than our nearly periodic modelled seismic cycles for full  
 543 ruptures. This may reflect incomplete long-term records (e.g., Lombardi et al., 2025; Mouslopoulou et al., 2025),  
 544 temporal changes in slip rates documented by cosmogenic dating (Benedetti et al., 2013; Cowie et al., 2017;  
 545 Mildon et al., 2022; Roberts et al., 2024, 2025; Sgambato et al., 2025), the greater geometrical complexity of  
 546 natural faults, and possibly also a larger ratio  $W_s/L_\infty$  (Barbot, 2019; Cattania, 2019), all of which could enhance  
 547 stress heterogeneity and variability.

548 While our models reproduce the magnitude range of historical single-fault events, they do not produce multi-fault  
 549 ruptures as documented in the historical catalogue in the region (Benedetti et al., 1998; Cello et al., 2003; Galli et

Formatted: English (UK)

550 al., 2006). This likely stems from the quasidynamic approximation, which does not simulate dynamic triggering  
551 by seismic waves and limits stress drops, slip velocities and rupture jumping compared to fully-dynamic  
552 simulations (Thomas et al., 2014). However, studies using other quasidynamic simulators (e.g. RSQSim, Dieterich  
553 and Richards-Dinger, 2010) have reported multi-fault rupture scenarios (Herrero-Barbero et al., 2021; Milner et  
554 al., 2021; Shaw et al., 2025). In these models, faults are more closely spaced and subject to higher effective normal  
555 stresses than our QDYN simulations (~100 MPa), which increases rupture energy favouring multi-fault ruptures.  
556 In addition, model approximations of RSQSim, such as discrete state transitions and prescribed slip rates during  
557 the sliding stage (Shaw et al., 2025) might also promote larger ruptures. In comparison, our simulations resolve  
558 continuous rate-and-state friction, and include velocity strengthening barriers at fault tips and lower effective  
559 normal stress, all of which would favour rupture arrest at the fault boundaries. This limitation likely leads to an  
560 underestimation of the largest seismic events and biases the upper tail of the magnitude-frequency distribution  
561 toward single-fault ruptures. While non-periodic multi-fault ruptures would likely increase the recurrence  
562 variability and cycle complexity of individual faults, it is not expected to change the first-order role of fault  
563 network geometry identified here. Multi-fault ruptures could be promoted by stronger velocity weakening  
564 asperities or higher normal stresses, but such parameter choices would increase the computational cost, limiting  
565 their feasibility in these regional-scale simulations. A second alternative to address this would be using simulated  
566 cycles as initial conditions for fully dynamic rupture models (Galvez et al., 2020).

Deleted: which

Deleted: (

567 Despite these limitations, our results show that SEAS models can capture key behaviours of complex fault  
568 networks and generate synthetic earthquake catalogues that are directly comparable with paleoseismic data. This  
569 provides a strong basis for future simulations integrating more geologically realistic features, such as along-strike  
570 variations of slip rate and strike.

## 571 5.2 Effect of stress redistribution within a fault network on simulated seismic sequences

572 Our simulations show that earthquakes on networks with multiple across-strike faults, such as those in the Central  
573 Apennines, generate spatially heterogeneous stress perturbations on nearby faults. These interactions promote  
574 more partial ruptures, greater variability in rupture lengths, magnitude and nucleation locations, and less periodic  
575 behaviour of large earthquakes. In contrast, faults within more along-strike networks, like in the Southern  
576 Apennines, experience more uniform stress loading and tend to produce more periodic and characteristic seismic  
577 cycles, behaviours more similar to simulations of isolated faults (Figs. 4a, 12,13). These results build upon prior  
578 numerical modelling work of (Rodriguez Picada et al., 2025a), which showed that complex and non-periodic  
579 seismic cycles emerge in a system of two across-strike normal faults. They also extend prior CST modelling work  
580 (Sgambato et al., 2020b, 2023), which showed that relatively isolated faults experience more regular stress loading  
581 histories dependent on interseismic loading than networks with multiple faults arranged across-strike.

Deleted: and

Deleted:

582 The effects of fault network geometry can be isolated when other factors such as long-term slip rate are considered  
583 constant. A clear example of the influence of fault network geometry comes from the Central Apennines, where  
584 the Scanno and Monte Marsicano faults have similar slip rates (Table 1), yet they have contrasting seismic cycle  
585 characteristics. The Monte Marsicano fault exhibits more irregular rupture timing, partial ruptures and rupture  
586 extent variability than the Scanno fault (Fig. 12), likely due to the influence of multiple closely-spaced CST

594 sources (Maiella, Sulmona, Scanno and Trasacco, Fig. E2e,f; E4, Appendix E), and therefore higher across-strike  
595 interaction index.

596 Fault networks also show longer recurrence times and larger magnitudes of full-rupture events, than the same  
597 faults modelled in isolation (Fig. 11). This results from stress interactions delaying full ruptures, allowing more  
598 time for fault healing and strength recovery, which leads to larger stress drops and higher seismic moments.  
599 Consequently, the magnitude versus rupture length scaling for fault networks (Fig. 8) better matches natural  
600 variability (Wells and Coppersmith, 1994), indicating that stress interaction among faults may contribute to the  
601 scatter seen in empirical scaling relationships.

602 Although not included in the simulations, the Parasano-Pescina, Tremonti and San Sebastiano may  
603 influence the seismic sequences of the Central Apennines fault network. Due to their limited area, the  
604 Parasano-Pescina and Tremonti faults would likely produce full-rupture events, similar to the Irpinia  
605 Antithetic fault in the Southern Apennines (Figure 4a-c). The inclusion of these tree faults would  
606 increase the number of across-strike interacting fault segments, thus promoting more stress  
607 heterogeneities in neighbouring faults such as Fucino, Scanno and Trasacco, and potentially leading to  
608 more complex seismic cycles or multi-fault ruptures. Given the limitations of the modelling framework,  
609 it is currently not feasible to investigate these interactions within a network-wide approach.

Deleted: ¶

610 Our focus is on normal fault networks, thus a remaining question is whether the findings will be applicable to  
611 strike-slip and thrust faults. We speculate that similar effects could occur in these settings, with the outcome  
612 depending on the degree of development of the fault network. Fault networks in late stage of development tend to  
613 evolve into more localized structures, reducing the fault overlap and the extent of interactions. In contrast,  
614 interaction effects may be more pronounced in early-stage networks, where a higher number of closely spaced  
615 overlapping faults are more common.

### 616 **5.3 Role of long-term slip rate in stress interaction effects**

617 When faults have few stress interactions with others, as in the Southern Apennines, their seismic cycle is primarily  
618 controlled by their long-term slip rate, with faster moving-faults having shorter recurrence times than slower-  
619 moving faults (Fig. G1, Appendix G).

620 In both Central and Southern Apennines, faults with higher long-term slip rates are more responsive to positive  
621 stress perturbations from nearby faults. For a given across-strike interaction index, faster-loading faults show less  
622 periodic recurrence of full ruptures and more variable rupture lengths (Fig. 12). Indeed, as these faults approach  
623 failure more often, they are more likely to be triggered by even small CST perturbations from nearby faults (e.g.,  
624 Sulmona, Liri and Trasacco faults in Central Apennines, Fig. 12). In contrast, slower-loading faults, such as the  
625 Volturara fault in the Southern Apennines (Fig. 7a), accumulate stress more slowly, experience stronger healing  
626 and show more regular recurrence.

627 This finding partially contrasts with results of elastic-brittle lattice models (e.g. Cowie et al., 2012), which  
628 associate higher CV with slower long-term slip rates in faults with multiple across-strike interactions. In those

630 models the absence of time-dependent stress healing means that slower loading allows heterogeneity to  
631 accumulate over longer timescales, increasing CV. In our rate-and-state friction models, by contrast, we isolate  
632 loading-rate effects at a fixed network geometry and find that CV increases with higher slip rate, consistent with  
633 reduced interseismic healing for the same time interval and higher sensitivity to small CST perturbations.  
634 Although the long-term slip-rate trends differ, both approaches agree that more complex fault networks lead to  
635 greater recurrence variability.

#### 636 5.4 Implications of fault network geometry on seismic hazard assessment

637 Physics-based earthquake simulators based on SEAS models provide an alternative framework to constrain  
638 earthquake rates and magnitude-frequency distributions for seismic hazard assessment (SHA, e.g., Milner et al.,  
639 2021; Shaw et al., 2018, 2022). To explore this potential, we compare magnitude-frequency distributions derived  
640 from our SEAS simulations with those obtained from an approach (Pace et al., 2016) based on seismic moment  
641 conservation and a truncated Gutenberg-Richter distribution (“fault-based method”, Appendix H).

Deleted: {Citation} {Citation}

642 For both fault networks, the two approaches yield systematically different magnitude-frequency distributions (Fig.  
643 4c.f). The fault-based method predicts lower recurrence rates than the SEAS simulations for  $M_w < 6.3$ , but higher  
644 rates at larger magnitudes. One likely explanation is that, unlike the fault-based method which assumes that the  
645 entire long-term slip rate is released seismically, the SEAS models allow part of the moment budget to be  
646 accommodated aseismically through creep or slow slip transients (e.g. Fig. 5c), thereby reducing the seismic  
647 budget for small earthquakes (Rodríguez Picada et al., 2025c). Additionally, the tested frictional properties in our  
648 SEAS models yield a  $W_s/L_\infty$  ratio (Eq. A5) that may favour more characteristic rupture behaviour, limiting the  
649 occurrence of smaller events relative to Gutenberg-Richter assumptions (Barbot, 2019; Cattania, 2019).

Deleted: (Rodríguez Picada et al., 2026b)(Rodríguez Picada et al., 2025c)

650 At the high-magnitude end, SEAS simulations produce larger magnitudes and higher rate of events than the fault-  
651 based method. This difference is likely due to the fault-based method assuming stationary recurrence and a priori  
652 prescribed maximum magnitude (Pace et al., 2016), while in the SEAS models rupture sizes emerge dynamically  
653 from stress evolution over a finite catalogue duration. Therefore, this comparison, although limited, shows how  
654 physics-based models can provide independent constraints both on the shape of the magnitude-frequency  
655 distribution and the maximum magnitude for SHA.

656 Beyond these general applications, our results also show how fault-network geometry modulates earthquake  
657 recurrence and magnitude variability challenging the common practice of applying uniform recurrence parameters  
658 (e.g. a single mean recurrence time or coefficient of variation) across an entire fault system (e.g., Nishenko and  
659 Buland, 1987; Ellsworth et al., 1999; Matthews et al., 2002). In networks with numerous across-strike faults and  
660 high long-term slip rates, recurrence can vary greatly between faults (e.g., Central Apennines, Fig. 9b),  
661 suggesting that hazard models should allow for broader epistemic uncertainty in recurrence and magnitude  
662 distributions. Therefore, probabilistic SHA could further benefit from integrating network-derived metrics, such  
663 as the across-strike interaction index, as quantitative guides for weighting logic-tree branches. While such metrics  
664 do not directly prescribe recurrence or magnitude parameters, they may provide physically grounded constraints  
665 to better reflect the complexity of fault interactions. Physics-based simulators are well suited to quantify the  
666 recurrence and magnitude variability (Milner et al., 2021; Shaw et al., 2018, 2022), and to inform the weighting

Formatted: Normal, Left, Line spacing: single

Moved (insertion) [1]

670 of alternative fault-based SHA models. In addition, time-dependent SHA approaches, such as those based on  
 671 Coulomb stress transfer histories (Chan et al., 2010; Iacoletti et al., 2021; Mignan et al., 2018; Stein et al., 1997;  
 672 Toda et al., 1998), should also account for spatial variability in stress changes. Finally, our simulations indicate  
 673 that overlap zones between faults can act as preferred nucleation sites and constrain rupture extent (Fig. 7),  
 674 highlighting their importance for assessing rupture scenarios and directivity effects (Spagnuolo et al., 2012;  
 675 Thompson and Worden, 2017).

## 676 6 Conclusions

677 We numerically simulated seismic cycles on two fault networks in the Southern and Central Apennines to examine  
 678 how changes in stress interactions caused by fault network geometry influence earthquake recurrence rates and  
 679 magnitudes. Increased number of fault interactions leads to a greater departure from the characteristic and periodic  
 680 behaviour of an isolated fault, with higher variability of earthquake recurrence, nucleation location and magnitude  
 681 with increasing fault interaction. Fault networks with multiple across-strike faults are characterised by more  
 682 complex seismic cycles than networks with fewer across-strike faults. When the number of across-strike  
 683 interactions is similar, faults with higher slip rates tend to produce less-periodic earthquakes with more variable  
 684 magnitude, meaning that slip rate influences how faults respond to stress changes from nearby ruptures. Our  
 685 models demonstrate that, by carefully considering the numerical limitations, simulated earthquake catalogues can  
 686 be meaningfully compared to natural earthquake records, highlighting the potential of using earthquake cycle  
 687 modelling to assess the seismic hazard of complex normal fault networks.

688

689

## 690 Appendix 1: SEAS governing equations and material properties

691 Fault friction follows the rate-and-state friction law (Dieterich, 1979; Marone, 1998a; Ruina, 1983), where the  
 692 shear stress ( $\tau$ ) along the fault is equal to its frictional strength:

$$693 \tau = \mu\sigma(A1)$$

694  $\mu$  is the coefficient of friction and  $\sigma$  is the effective normal stress (total normal stress minus pore-fluid pressure).  
 695 We adopt the regularised formulation of rate-and-state (Lapusta et al., 2000; Rice and Ben-Zion, 1996) where  
 696 friction evolves with slip rate ( $V$ ) and a state variable ( $\theta$ ) as:

$$697 \mu(\theta, V) = a \sinh^{-1} \left[ \frac{V}{2V^*} \exp \left( \frac{\mu^* + b \ln \left( \frac{V^* \theta}{D_c} \right)}{a} \right) \right] \quad (A2)$$

698 where  $\mu^*$  is the reference coefficient of friction at a reference slip rate  $V^*$ ;  $a$  and  $b$  are constants for the magnitude  
 699 of the contributions of the slip rate and fault state to the friction, respectively.  $D_c$  is the characteristic slip distance  
 700 and it controls how the state variable evolves following the aging law (Dieterich, 1979; Ruina, 1983):

Formatted: English (UK)

**Moved up [1]:** (e.g., Nishenko and Buland, 1987, Ellsworth et al., 1999; Matthews et al., 2002). In systems with numerous across-strike faults and high long-term slip rates, CV values can vary greatly between individual faults, suggesting that hazard models should use broader recurrence and magnitude-frequency distributions to reflect more irregular earthquake behaviour. Probabilistic SHA could further benefit from integrating network-derived metrics, such as the across-strike interaction index, into logic tree weights to better capture the seismic cycle complexity. In addition, time-dependent SHA models based on CST history (Chan et al., 2010; Iacoletti et al., 2021; Mignan et al., 2018; Stein et al., 1997; Toda et al., 1998) should also account for spatial variability in stress changes, which can affect the earthquake recurrence, a limitation increasingly addressed by physics-based earthquake simulators (Milner et al., 2021; Shaw et al., 2018, 2022). Finally, our simulations indicate that overlap zones between faults can act as preferred nucleation sites and constrain rupture extent (Fig. 7), highlighting their importance for assessing rupture scenarios and directivity effects (Spagnuolo et al., 2012; Thompson and Worden, 2017).  
 Overall, our study highlights how, by carefully considering the limitations, meaningful earthquake cycle statistics and the evolution of stress can be explored using SEAS simulations across complex fault networks, providing useful inputs into seismic hazard assessments of actively extending regions like Italy.

**Deleted:** The fact that fault network geometry influences variability in earthquake recurrence and magnitude within a fault system challenges the common practice in time-dependent seismic hazard assessment (SHA) of applying a single mean recurrence time and coefficient of variation across the entire network (e.g., Nishenko and Buland, 1987, Ellsworth et al., 1999; Matthews et al., 2002). In systems with numerous across-strike faults and high long-term slip rates, CV values can vary greatly between individual faults, suggesting that hazard models should use broader recurrence and magnitude-frequency distributions to reflect more irregular earthquake behaviour. Probabilistic SHA could further benefit from integrating network-derived metrics, such as the across-strike interaction index, into logic tree weights to better capture the seismic cycle complexity. In addition, time-dependent SHA models based on CST history (Chan et al., 2010; Iacoletti et al., 2021; Mignan et al., 2018; Stein et al., 1997; Toda et al., 1998) should also account for spatial variability in stress changes, which can affect the earthquake recurrence, a limitation increasingly addressed by physics-based earthquake simulators (Milner et al., 2021; Shaw et al., 2018, 2022). Finally, our simulations indicate that overlap zones between faults can act as preferred nucleation sites and constrain rupture extent (Fig. 7), highlighting their importance for assessing rupture scenarios and directivity effects (Spagnuolo et al., 2012; Thompson and Worden, 2017).  
 Overall, our study highlights how, by carefully considering the limitations, meaningful earthquake cycle statistics and the evolution of stress can be explored using SEAS simulations across complex fault networks, providing useful inputs into seismic hazard assessments of actively extending regions like Italy.

762 
$$\frac{d\theta}{dt} = 1 - \frac{V\theta}{D_c} \quad (A3)$$

763 At steady state,  $\frac{d\theta}{dt} = 0$ , so steady state-friction is:

764 
$$\mu_{ss} = a \sinh^{-1} \left[ \frac{V}{2V^*} \exp \left( \frac{\mu^* + b \ln(\frac{V}{V^*})}{a} \right) \right] \quad (A4)$$

765 In this state, the parameter  $(a - b)$  describes the dependence of  $\mu_{ss}$  with velocity, with positive  $(a - b)$   
 766 characteristic of velocity-strengthening materials (i.e. steady-state friction increases with increasing velocity) and  
 767 negative  $(a - b)$  characteristic of velocity-weakening materials (i.e. steady-state friction decreases with  
 768 increasing velocity). Velocity-weakening materials can develop stick-slip behaviour, thus they are assumed to be  
 769 characteristic of the seismogenic portion of a fault or seismic asperity. To produce unstable sliding, the smallest  
 770 dimension (length  $L$  or width  $W$ ) of a segment with velocity strengthening material must exceed a so-called  
 771 nucleation length ( $L_\infty$ ) (Rubin and Ampuero, 2005):

772 
$$L_\infty = \frac{1}{\pi} \left( \frac{b}{b-a} \right)^2 \frac{GD_c}{b\sigma} \quad (A5)$$

773 where  $G$  is the shear modulus of the host rock. If the size of the velocity-weakening fault does not exceed the  
 774 nucleation length, aseismic slip will occur (Rubin and Ampuero, 2005).

775 To compute earthquake cycles, QDYN solves the equation of elasto-static equilibrium, where stress and slip rate  
 776  $V$  are related by (Rice, 1993):

777 
$$\tau_0 + \tau_e - \frac{G}{2c} V = \sigma \mu \quad (A6)$$

778 where  $\tau_0$  is the background shear stress,  $\tau_e$  is the elastic shear stress due to fault slip,  $\frac{G}{2c}$  is the radiation damping  
 779 term which approximates the inertial effects of seismic waves,  $c$  is the shear-wave speed,  $\sigma$  is the effective normal  
 780 stress, calculated by summing the initial normal stress  $\sigma_0$  and the elastic normal stress  $\sigma_e$  from stress interactions:

781 
$$\sigma = \sigma_0 + \sigma_e \quad (A7)$$

782 QDYN utilises the back-slip approach, such that the stresses transmitted from a fault element to neighbouring  
 783 elements are proportional to their slip deficit relative to the long-term tectonic slip (Heimisson, 2020; Savage,  
 784 1983). In this interpretation of backslip, faults are approximately modelled as faults of finite size loaded remotely  
 785 by tectonic stresses (Allam et al., 2019; Dieterich and Smith, 2010). When faults are remotely loaded in an elastic  
 786 medium, they tend to accumulate stresses indefinitely with increasing slip; however, due to the crust finite  
 787 strength, there should be some process of off-fault inelastic deformation to relax these stresses. The backslip  
 788 method approximately accounts for these inelastic processes, such that it maintains kinematic consistence with  
 789 the long-term slip rate of faults (Allam et al., 2019; Dieterich and Smith, 2010). The backslip approach  
 790 implemented in QDYN is the same as in Heimisson (2020).

791 The elastic shear stress at the  $i$ -th fault element  $\tau_i^e$  due to the slip on the remaining fault elements is:

$$792 \tau_i^e = - \sum_j k_{ij}^t (u_j(t) - V_{PL}t) \quad (A8)$$

793 where  $V_{PL}$  is the long-term tectonic slip rate on the fault,  $u_j$  is the slip on the  $j$ -th cell and  $k_{ij}^t$  is the stiffness matrix  
794 for shear stress, which describes the shear stress change on the  $i$ -th fault element exerted by a unit slip on the  $j$ -th  
795 fault element. The elastic normal stress  $\sigma_e$  from Eq. A7 is calculated similarly than in Eq. A8, but with the stiffness  
796 matrix for normal stress  $k_{ij}^\sigma$ :

$$797 \sigma_i^e = - \sum_j k_{ij}^\sigma (u_j(t) - V_{PL}t) \quad (A9)$$

799 Both stiffness matrices in eqs. A8 and A9 are calculated using the analytical equations for static stresses induced  
800 by rectangular dislocations in a homogeneous elastic half-space (Okada, 1992). Free surface conditions are  
801 included in the formulations. Because the faults have varying orientations relative to one another, we are unable  
802 to use optimizations that take advantage of the invariant strikes to construct the stiffness matrices, such as Fast  
803 Fourier transforms (Rice, 1993). Instead, we use the implementation by Galvez et al., (2020) of the hierarchical  
804 matrix (H-matrix) compression to the stress transfer component (Bradley, 2014) and the LSODA solver  
805 implemented by Yin et al. (2023). Despite the improved time-stepping efficiency demonstrated in Yin et al.  
806 (2023), the simulations remain computationally demanding, requiring approximately two months to complete.

807 The material and frictional properties are listed in Table A1. Each fault consists of a rectangular patch in the centre  
808 with velocity-weakening properties, bounded by a velocity-strengthening region with a width of 1.5 km in the  
809 Southern Apennines and 1.1 km in the Central Apennines. Additionally, we set a 1 km transition zone with  
810 velocity-strengthening friction properties along the edges of the velocity-weakening regions to prevent infinite  
811 stress rates at the fault edges that could arise from the backslip method (Rodriguez Piceda et al., 2025a).

812 The variation of normal stress with depth follows the approach by Lapusta et al. (2000), where effective normal  
813 stress  $\sigma_t$  equals the lithostatic pressure minus the hydrostatic pore-fluid pressure at shallow depths, with a  
814 transition to lithostatic pore pressure gradient with a 50 MPa offset at depth ( $z$ ):

$$815 \sigma_t = \min \left\{ \begin{array}{l} 2.8 + 18 * z / km \\ 50 MPa \end{array} \right. \quad (A10)$$

816 We account for the dip angle of the normal faults ( $\alpha$ ) in our simulations:

$$817 \sigma = \sigma_t \sin(\alpha) \quad (A11)$$

818 In this set up, where multiple faults are interacting, the normal stress can reach negative values near the surface.  
819 To accommodate the possible stress change that could occur during the spin-up phase, the initial minimum normal  
820 stress is increased to 15 MPa (Yin, 2022).

**Deleted:** Additionally, a 1 km transition zone was set between the velocity-strengthening and the velocity-weakening and regions

**Deleted:** {Citation} {Citation} {Citation}.

825

826 **Table A1:** Material and frictional properties of the model set up in the Central Apennines (CA) and Southern  
827 Apennines (SA).

Symbol	Description (units)	Value
G	Shear modulus (GPa)	32
$\lambda$	Elastic modulus (GPa)	32
c	Shear wave velocity (m/s)	3000
$\mu^*$	Reference friction coefficient	0.6
$a$	Direct-effect parameter	0.007
$b$	Evolution effect parameter	0.014 (VW) / 0.0042 (VS)
$D_c$	Characteristic slip distance (mm)	8 (SA), 10 (CA)
$V_{PL}$	loading rate	see table 1
$V^*$	Reference slip rate (m/s)	$=V_{PL}$
$V_0$	Initial slip rate (m/s)	$0.8 V_{PL}$
$D_w, D_x$	Cell size along-dip (m), Cell size along-strike (m)	110 (SA), 128 (CA)

Deleted: □

Deleted: A

Deleted: B

Formatted: Subscript

828 **Appendix B: Historical and paleoseismicity of the Southern and Central Apennines**

829 **Table B1:** Historical seismic events (>0A.D.) based on (Mildon, 2017a; Sgambato, 2022). \*Magnitudes of  
830 seismic events in Central Apennines prior to 1979 A.D. are taken from the Catalogue di Forti Terremoti  
831 (Guidoboni et al., 2019) and are derived from the macroseismic shaking records (Gasperini and Ferrari,  
832 2000) and as such are described as equivalent magnitudes ( $M_e$ , based on Mildon, 2017). For more recent

836 earthquakes in the Central Apennines post 1979 A.D. the magnitudes described are from seismological  
837 sources. <sup>1</sup>The name NW segment of Vallo di Diano often differs in the literature, being also known as  
838 Auletta fault or Caggiano fault (Bello et al., 2022; Galli et al., 2006a)

Earthquake Date	Magnitude*	Source Fault	Proportion of the fault that slips	Reference
<b>Southern Apennines</b>				
15/01/1466	5.98	Irpinia	SE section 13 km	Marturano (2007)
31/07/1561	6.1	San Gregorio	Entire fault	Castelli et al. (2008)
19/08/1561	6.4-6.5	Vallo Di Diano <sup>1</sup>	all	Galli et al. (2006)
08/09/1694	6.73	Irpinia	All	Galli et al., (2006, 2014); Galli and Peronace (2014)
01/02/1826	5.74	Val d'Agri	Northern section 10 km	Rovida et al., (2020)
09/04/1853	5.6	Irpinia	Northern section 8 km	Galli and Peronace, (2014)
16/12/1857	7.12	Vallo di Diano and Val D'Agri	Northern section Vallo Di Diano (12km) + entire Val D'Agri	Benedetti et al., (1998); Cello et al. (2003); Galli et al. (2006)
07/06/1910	5.76	Irpinia Antithetic	Entire fault	Galli and Peronace (2014)
		Irpinia	Southern section of Irpinia (10 km)	
23/11/1980	6.81	Irpinia, San Gregorio? and Irpinia antithetic	Entire faults	Galli and Peronace (2014); Giardini et al. (1996); Rovida et al. (2020); Sgambato et al. (2025); Westaway, (1993); Westaway and Jackson (1987)
<b>Central Apennines</b>				

05/12/1456	5.8	Sulmona	Northern section (9km)	Guidoboni et al. (2019)
24/07/1654	6.3	Liri and Fibreno	Southern section of Liri (13 km) + entire Fibreno fault (6.6 km)	
3/11/1706	6.8	Maiella	Entire fault	Guidoboni et al. (2019)
		Maiella and Palena	Entire faults	
13/01/1915	7	Fucino, Parasano and San Sebastiano	Entire faults	Michetti et al. (1996)
		Fucino, Luco and Trasacco	Entire Fucino and Luco faults + northern section of Trasacco (8km)	
26/09/1933	6	Maiella	Central section (12.2 km)	Pizzi et al. (2010)

Deleted: s

839

840 **Table B2: Paleoearthquakes and historical events in modelled faults of the Southern and Central**  
841 **Apennines. The nomenclature of some of the faults adopted by Faure Walker et al. (2021) and Sgambato**  
842 **et al. (2020) and in this study differs from that of the paleoseismic data: <sup>1</sup>part of the Monte Marzano fault**  
843 **system by Galli (2020); <sup>2</sup>part of this fault is the San Benedetto dei Marsi–Gioia dei Marsi segment in the**  
844 **Fucino fault system in Galadini and Galli (1999); <sup>3</sup>also known as Monte Morrone fault by Galli et al. (2015).**  
845 **Paleoevents in bold are events with defined aged brackets used for the calculations of mean and standard**  
846 **deviation of recurrence times in the Discussion section.**

Fault	N Paleoevents	Date of paleoevents	Reference
<b>Southern Apennines</b>			
Irpinia <sup>1</sup>	5	<b>6736-8600 B.P.; 4411-6736 B.P.; 3507-4283 B.P.; 1415-2754 B.P.; 1980 A.D.</b>  Pantano di San Gregorio Magno segment:	(D'Addezio et al., 1991; Pantosti et al., 1993)

		11,180–19,660 B.P., 6620–9420 B.P., 2570–6620 B.P., 1720–2570 B.P.; 1980 A.D	
<b>Central Apennines</b>			
Fucino-Ovindolli-Pezza <sup>2</sup>	6	20,000–32,520 ± 500 B.P.; 12,729–7,576 B.P.; 3,500–3,300 B.P.; 426–782 AD; 1231 AD; 1915 AD	Galadini and Galli (1996, 1999); Galli et al. (2016)
Sulmona <sup>3</sup>	6	Before 9,000 B.P.; 6,500–8,500 B.P.; 5,500 B.P.; 200 AD, 1456 AD	Galli et al. (2015)
Trasacco	7	After 12,600 B.P.; 12,600–12,000 B.P.; 7,000–6,600B.P.; 6,500–5,900B.P.; 3,500–3,600 B.P. to 3,400–3,500 B.P.; 1,500– 1,600B.P. or 1,500–1,400 B.P.; 1915 AD	Galadini and Galli, (1999)
Liri	3	Before 12,500 B.P.; before 5,000 B.P.; before 1,500 B.P.	Pace et al., (2020)

848 **Table B3: Comparison between recurrence times (mean and standard deviation in years) derived from**  
849 **historical and paleoseismological data ( $Tr_{paleo}$ ) and modelled seismic events ( $Tr_{model}$ ). Only paleoseismic**  
850 **events with well-defined age brackets were included in the calculation (see Table B2).  $Tr_{paleo}$  = recurrence**  
851 **times based on historical and paleoseismological data from the past 20 kyr. Scaled  $Tr_{model}$  = recurrence**  
852 **times from modeled seismic events adjusted by the correction factor.**

Formatted: English (UK)

<b>Fault</b>	<b><math>Tr_{paleo} \pm \sigma</math></b>	<b>Scaled <math>Tr_{model}</math></b>
Irpinia (SA)	1900 ± 186	454±161
Fucino (CA)	4253 ± 4465	900±720
Sulmona (CA)	1866±1231	1440±620
Trasacco (CA)	2469±1259	1217±290

Formatted: Font: (Default) Times New Roman, 10 pt, English (UK)

Formatted: Font: (Default) Times New Roman, 10 pt, English (UK)

Formatted: Font: (Default) Times New Roman, 10 pt, English (UK)

Formatted: Font: (Default) Times New Roman, 10 pt, English (UK)

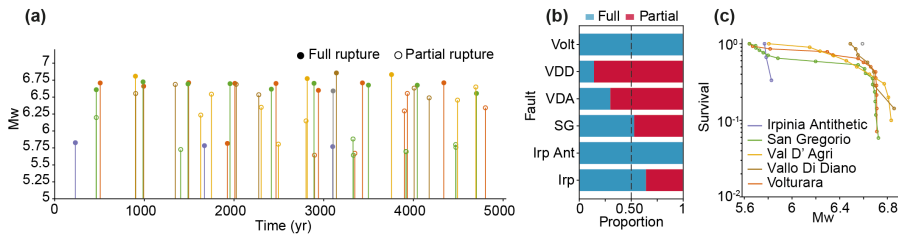
Formatted: Font: (Default) Times New Roman, 10 pt, English (UK)

Formatted: Font: (Default) Times New Roman, 10 pt, English (UK)

Formatted: Font: (Default) Times New Roman, 10 pt, English (UK)

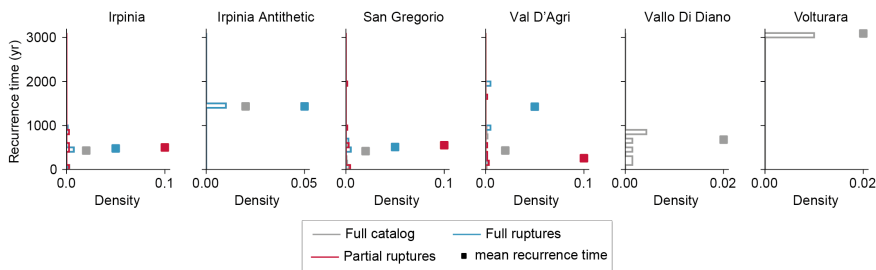
853

854 **Appendix C: SEAS simulations of Southern Apennines with nominal slip rate**



855  
 856 **Figure C1: synthetic catalog for a simulation of the Southern Apennines with nominal values of prescribed**  
 857 **long-term slip rate. (a) Time distribution of simulated full- and partial-rupture events with stems and**  
 858 **markers color-coded by fault (b) (b,e) proportion of full and partial ruptures per fault. (c) Magnitude-**  
 859 **frequency distributions of seismic events shown as survival function (number of events with a Mw larger**  
 860 **than a given value normalized by total number of events) for each fault. Color legend for each fault is shown**  
 861 **in panels (c).**

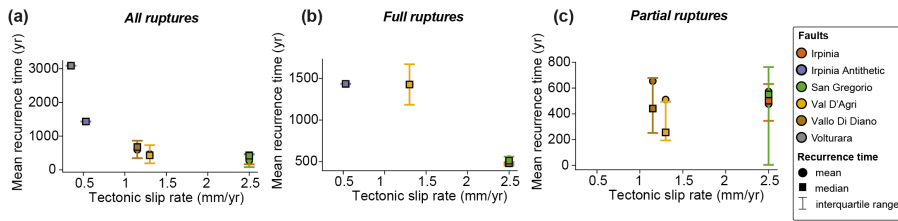
862



863  
 864 **Figure C2: Variation of recurrence time of individual faults (step density histogram and mean recurrence**  
 865 **time) and of the entire fault system for seismic events considering the full catalog, full-rupture and partial-**  
 866 **rupture events of the fault networks for a simulation of the Southern Apennines with nominal values of**  
 867 **prescribed long-term slip rate.**

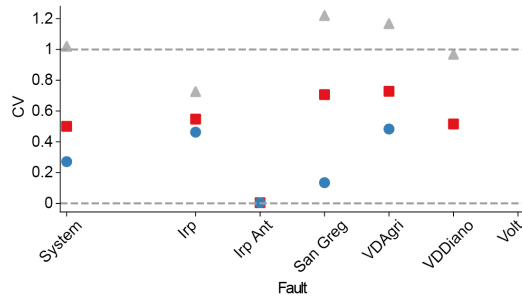
Formatted: English (UK)

868



869  
 870 **Figure C3: Mean, median and interquartile range of recurrence time of seismic events vs. (scaled) long-**  
 871 **term tectonic slip rate of individual faults for a simulation of the Southern Apennines with nominal values**  
 872 **of prescribed long-term slip rate.**

Formatted: English (UK)



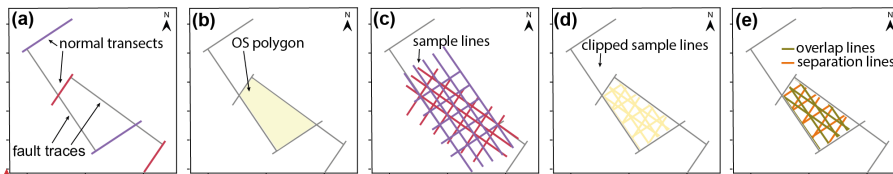
873

874 **Figure C4: Coefficient of variation of recurrence times  $CV_{Tr}$  of seismic events (all events, only full ruptures**  
 875 **and only partial ruptures) for individual faults and entire fault system for a simulation of the Southern**  
 876 **Apennines with nominal values of prescribed long-term slip rate.**

877

878 **Appendix D: Determination of separation between faults**

879 To determine the separation between two faults at depths of 0, 7.5 and 15 km we followed the following steps.  
 880 First, for all fault traces, we created bounding transects normal to the fault tips (Fig. D1a). Second, for each fault  
 881 pair, we drew a polygon bounded by two of the transects (one for each fault) and the fault traces (Fig. D1b). Third,  
 882 we created sample lines (separation lines) equally spaced by 100 m parallel to the transects (Fig. D1c). Lines that  
 883 did not intersect the fault traces or the transects were removed. Fourth, we clipped the sample lines to the polygon  
 884 area (Fig. D1d-e). Finally, for each set of overlap and separation lines, we computed the average length (preferred  
 885 value) and standard deviation. The workflow was carried out with QGIS (QGIS Development Team, 2009).

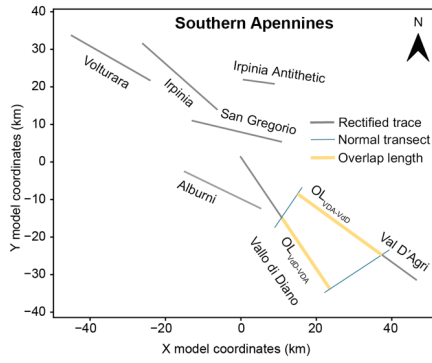


886

887 **Figure D1: illustrative workflow used to determine the separation between two fault traces at a given depth.**

**Deleted:** (Pace et al., 2016)(Hanks and Kanamori, 1979)(Pace et al., 2016)  
**Formatted:** Font: 12 pt

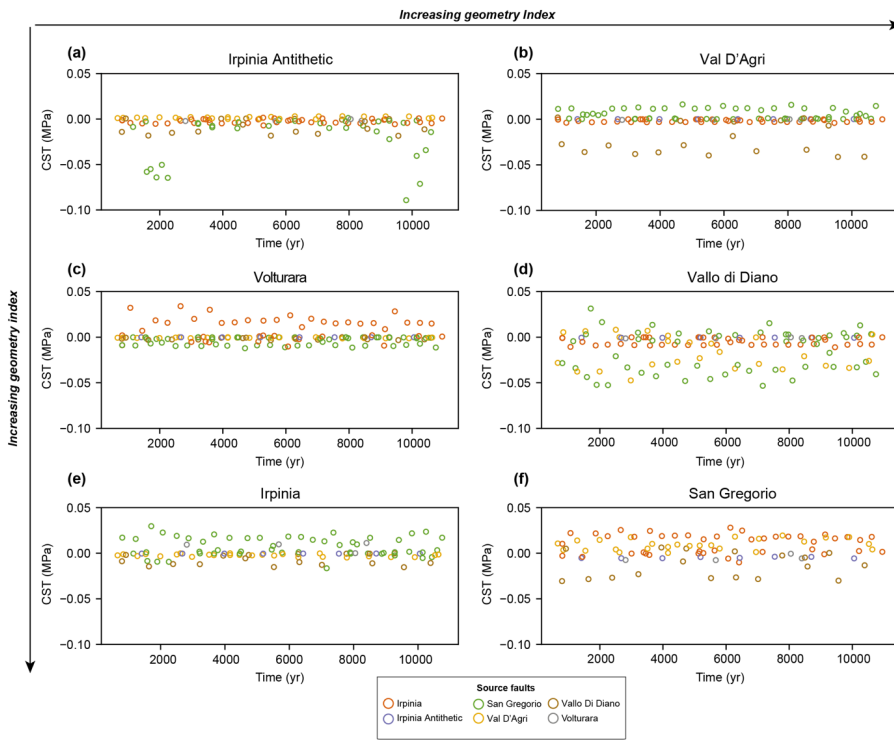
**Formatted:** English (UK)



890

891 **Figure D2: Determination of overlap length between two faults (in this example, Vallo Di Diano and Val**  
 892 **D'Agri fault in the Southern Apennines) used for Figure 7 and S7-S8. To determine the overlap length**  
 893 **between two given faults (fault 1 and 2), we measure the distance along the strike of fault 1 between the**  
 894 **normal transect to one of the tips of fault 1 to the normal transect of to one of the tips of fault 2.**

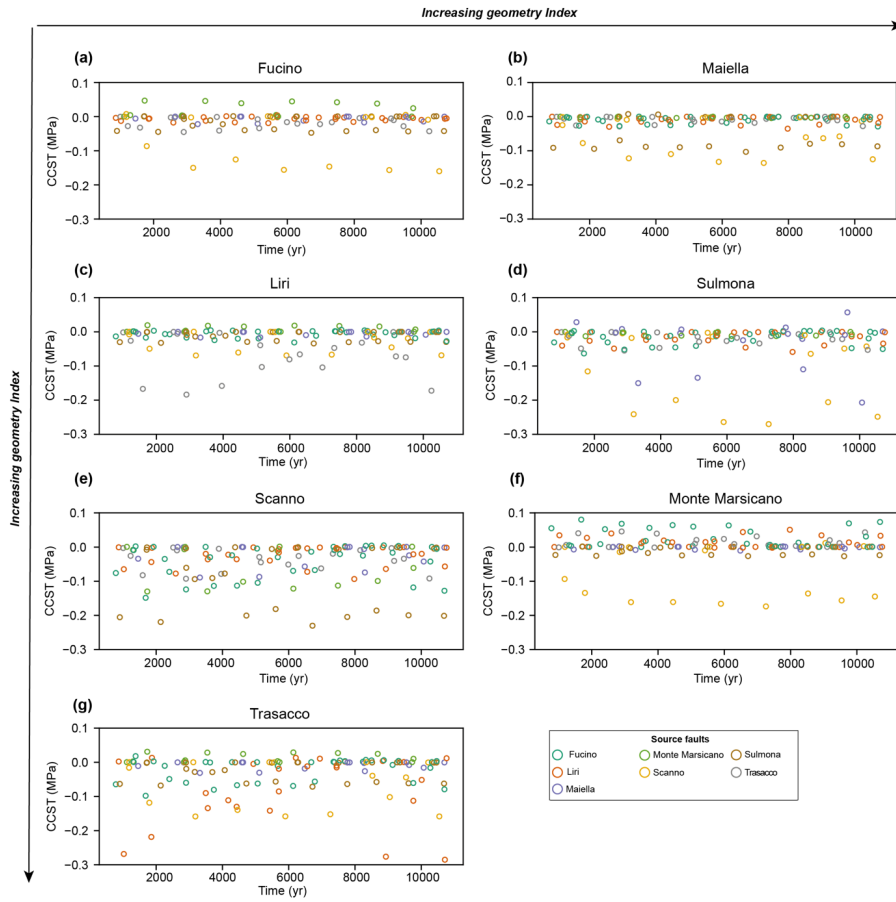
895 **Appendix E: Coseismic coulomb stress transfer**



896

897

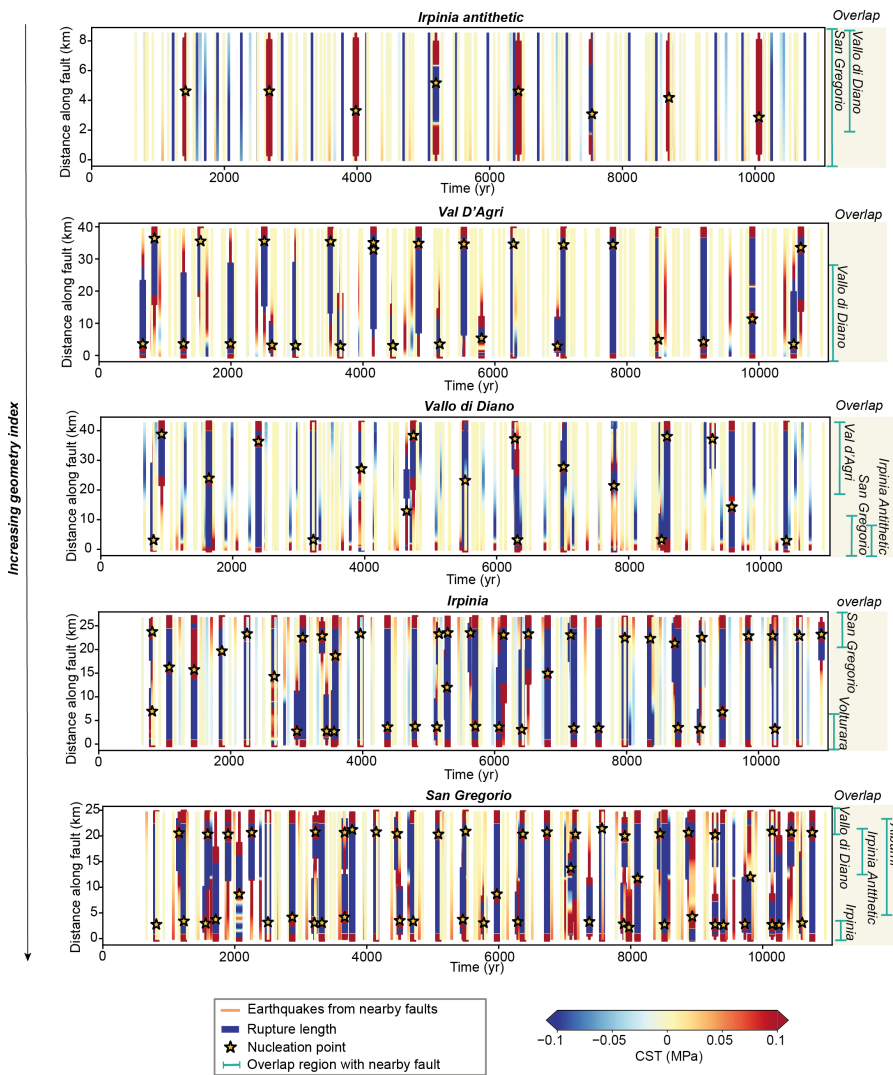
898 **Figure E1: Time series with coseismic Coulomb stress transfer (CST) averaged across the fault surface**  
899 **induced by nearby faults in the Southern Apennines.**



900

901

902 **Figure E2: Time series with coseismic stress transfer averaged across the fault surface induced by nearby**  
903 **faults in the Central Apennines.**



904

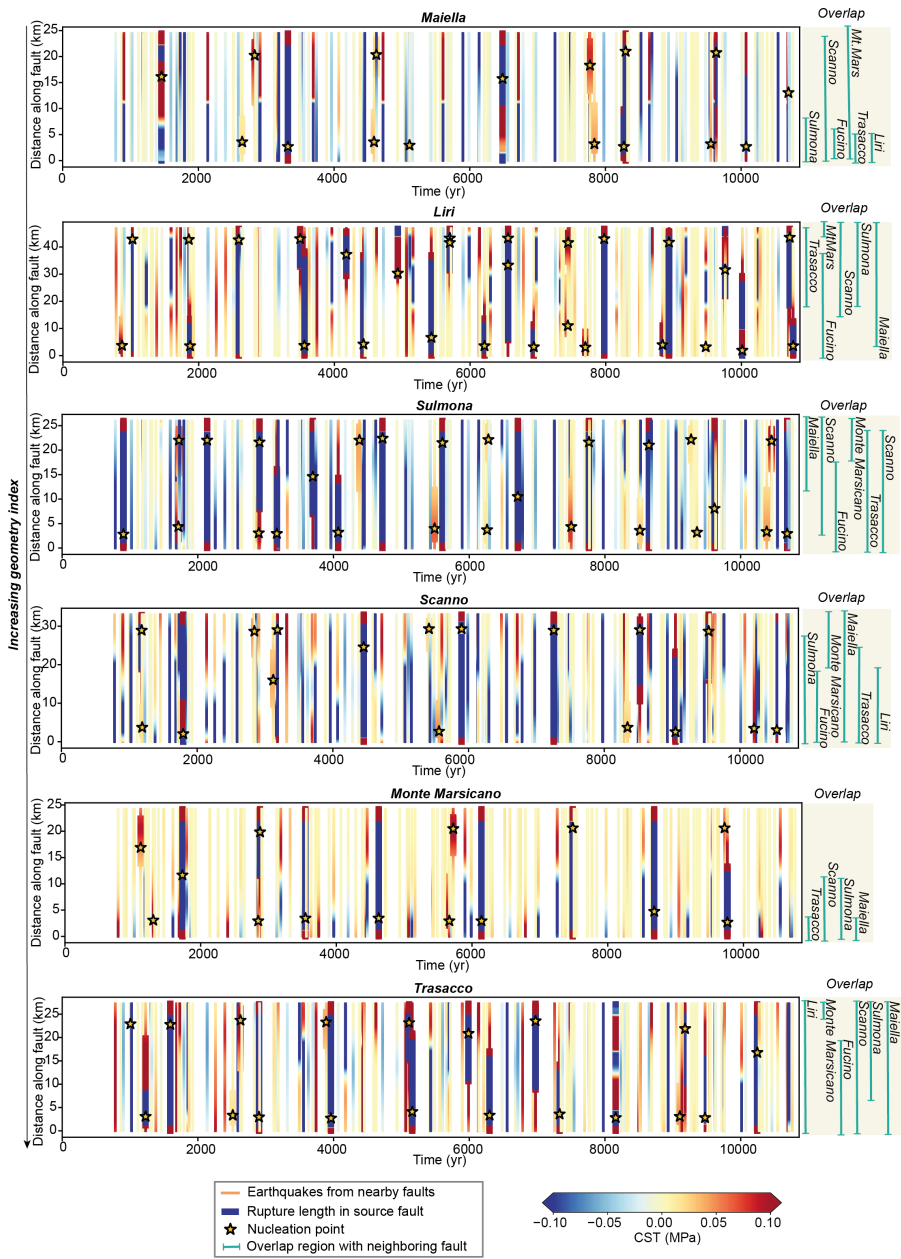
905 **Figure E3: Coseismic stress transfer (CST) in the Irpinia Antithetic, Val D'Agri, Vallo di Diano, Irpinia**  
 906 **and San Gregorio faults in the southern Apennines. For the figure explanation, see caption of Figure 8 in**  
 907 **the main text.**

908

909

910

911



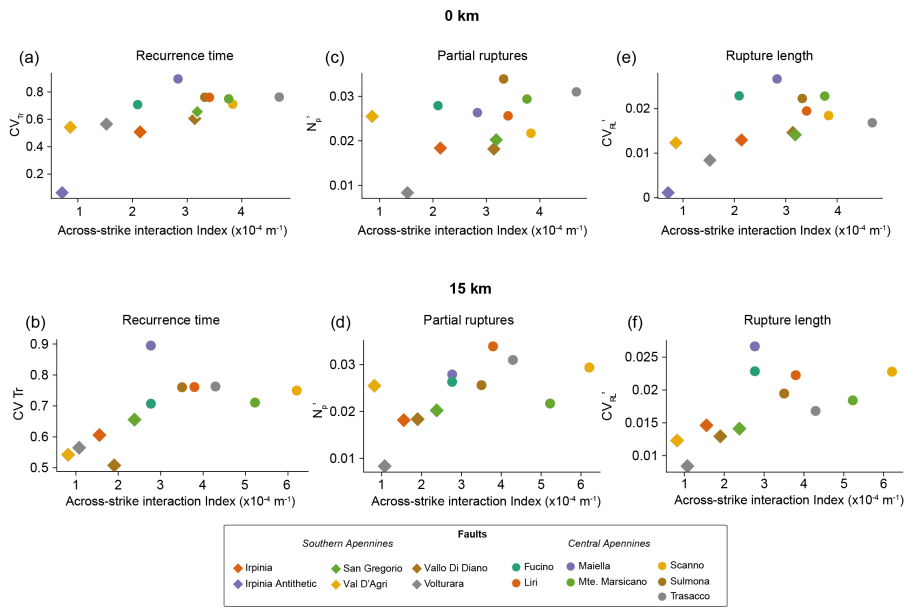
912

913

914 Figure E4: Coseismic stress transfer (CST) in the Maiella, Liri, Sumona, Scanno, Monte Marsicano and  
 915 Trasacco faults in the Central Apennines. For the figure explanation, see caption of Figure 8 in the main  
 916 text.

917

918 Appendix F: Across-interaction index



919

920 Figure F1: relationships between fault network geometry, described by the across-strike interaction index  
 921 (AI), and (a-b) coefficient of variation of recurrence times ( $CV_{Tr}$ ), (b-c) number of partial ruptures ( $N_p'$ )  
 922 and (d-e) coefficient of variation of rupture lengths ( $CV_{r_l}'$ ) for faults in the Southern and Central  
 923 Apennines. AI index corresponds to a depth of (a,d,e) 0 km and (b,d,f) 15 km.

924

925 Table F1: Leave-one-out Spearman's correlation coefficients (mean, standard deviation, minimum,  
 926 maximum) for relationship between across-strike interaction index (taken at 0 km, 7.5km and 15km) and  
 927 coefficient of variation of recurrence times ( $CV_{Tr}$ ), number of partial ruptures ( $N_p'$ ) and coefficient of  
 928 variation of rupture lengths ( $CV_{r_l}'$ ) for faults in the Southern and Central Apennines

Depth (km)	metric	Mean $\rho$	Std $\rho$	Min $\rho$	Max $\rho$
<b>Southern Apennines + Central Apennines</b>					
0	$CV_{Tr}$	0.72	0.05	0.64	0.85
	$N_p'$	0.46	0.08	0.34	0.58

Deleted: G

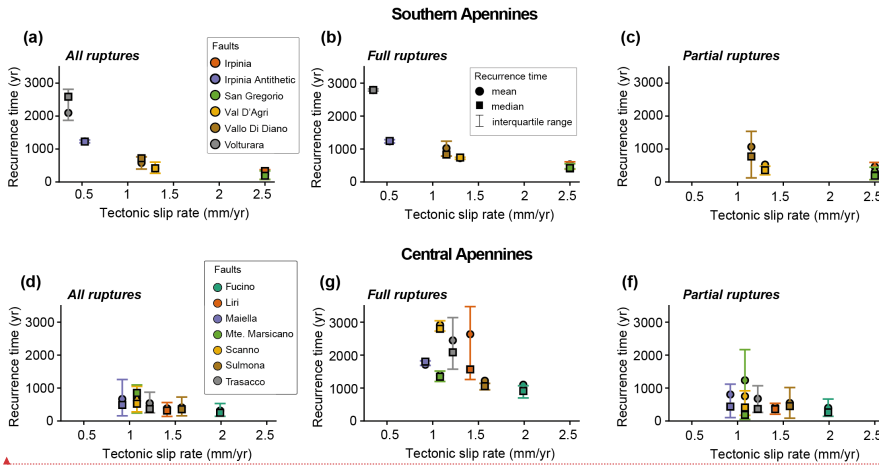
Formatted: Font colour: Text 1

	$CV_{rl}'$	0.50	0.09	0.37	0.67
7.5	$CV_{Tr}$	0.84	0.03	0.80	0.90
	$N_p'$	0.73	0.05	0.68	0.85
	$CV_{rl}'$	0.71	0.06	0.64	0.78
15	$CV_{Tr}$	0.70	0.06	0.62	0.81
	$N_p'$	0.69	0.06	0.65	0.85
	$CV_{rl}'$	0.66	0.07	0.57	0.75
<b>Southern Apennines only</b>					
0	$CV_{Tr}$	0.82	0.13	0.70	1.00
	$N_p'$	-0.08	0.50	-0.40	0.80
	$CV_{rl}'$	0.87	0.05	0.80	0.90
7.5	$CV_{Tr}$	0.40	0.42	-0.20	1.00
	$N_p'$	0.04	0.54	-0.20	1.00
	$CV_{rl}'$	0.56	0.17	0.40	0.80
15	$CV_{Tr}$	0.65	0.23	0.40	1.00
	$N_p'$	0.04	0.54	-0.20	1.00
	$CV_{rl}'$	0.75	0.10	0.60	0.90
<b>Central Apennines only</b>					
0	$CV_{Tr}$	0.09	0.28	-0.43	0.43
	$N_p'$	0.00	0.24	-0.37	0.31
	$CV_{rl}'$	-0.84	0.06	-0.94	-0.77
7.5	$CV_{Tr}$	-0.27	0.25	-0.71	0.14
	$N_p'$	0.13	0.22	-0.09	0.60
	$CV_{rl}'$	-0.56	0.20	-0.89	-0.31
15	$CV_{Tr}$	0.18	0.27	-0.31	0.54
	$N_p'$	0.31	0.18	0.09	0.60

	$CV_{rl}'$	-0.70	0.12	-0.89	-0.54
--	------------	-------	------	-------	-------

930

931 **Appendix G: Recurrence time and tectonic slip rate**



932

933 **Figure G1: Mean, median and interquartile range of recurrence time of seismic events vs. long-term**  
 934 **tectonic slip rate of individual faults for (a) Southern Apennines and (b) Central Apennines**

935 **Appendix H: Calculation of magnitude-frequency distributions with the moment budget method**

936 We estimate annual cumulative earthquake rates for individual faults and fault networks using the moment-budget  
 937 (MB) and activity-rate (AR) tools implement in the seismic-hazard code FiSH (Pace et al., 2016). This approach  
 938 is based on the conservation of seismic moment over tectonic time scales, requiring information of the fault  
 939 geometry and long-term slip-rate (Table 1). For each fault, the moment rate  $M_0$  that must be released by  
 940 earthquakes on the fault over time is calculated as:

941 
$$M_0 = GAD(H1)$$

942 Where  $G$  is the shear modulus,  $A$  is the fault area derived from its geometry and  $D$  is the long-term slip rate.  
 943 Earthquake magnitudes  $M_w$  are related to the seismic moment  $M_0$  through the standard relationship of Hanks and  
 944 Kanamori (1979):

945 
$$\log_{10}(M_0) = 1.5M_w + 9.1 (H2)$$

946 We used the truncated Gutenberg Richter formulation, where the incremental magnitude frequency distribution is  
 947 defined as:

948 
$$v(M) = C10^{-b(M-M_{min})}, M_{min} \leq M \leq M_{max} (H3)$$

Formatted: English (UK)

949 Where  $b$  is the b-value ( $b=1$ ),  $M_{min}$  the minimum magnitude ( $M_{min}=5.5$ ) and  $M_{max}$  the fault-specific maximum  
950 magnitude inferred from geometry. The constant  $C$  is determined by enforcing the moment conservation, such as  
951 the integral of the seismic moment released by the distribution is equal to the long-term moment rate:

$$952 \int_{M_{min}}^{M_{max}} M_0(M)v(M)dM = M_0 \text{ (H4)}$$

953 From the incremental rates, we calculate the annual cumulative exceedance rate for each fault defined as the  
954 expected annual number of events with magnitude equal or greater than  $m$ :

$$955 \lambda(M \geq m) = \int_m^{M_{max}} v(M)dM \text{ (H5)}$$

956 To obtain the exceedance rates per fault network, we summed the cumulative rates assuming independent  
957 Poissonian sources. Further details on this approach are provided in (Pace et al., 2016)

958

959

## 960 **Acknowledgements**

961 This research was funded by UK Research and Innovation (UKRI) under the auspices of the project QUAKE4D  
962 (MR/T041994/1) awarded to Zoë Mildon. This work was carried out using the computational facilities of the  
963 ARCHER2 UK National Supercomputing Service (<https://www.archer2.ac.uk>). J.P.A. was supported by the  
964 French government through the UCAJEDI Investments in the Future project (ANR-15-IDEX-01) managed by the  
965 National Research Agency (ANR). Y.Y. was supported by the Swiss National Science Foundation  
966 Postdoc.mobility Grant P500PN\_214179. We thank the two anonymous reviewers, whose comments helped to  
967 improve this manuscript.

Formatted: English (UK)

## 968 **Code and data availability**

969 Data to build the fault sources was taken from open-access publications (Faure Walker et al., 2019b; Mildon,  
970 2017b; Sgambato, 2022; Valentini et al., 2017). QDYN is open source (Luo et al. 2017). The modified code  
971 version used in this work can be found in (Rodriguez Piceda et al., 2025b). Input files to reproduce the results of  
972 this work are accessible in (Rodriguez Piceda et al., 2026).

Formatted: English (UK)

Formatted: English (UK)

## 973 **Competing interests**

974 The authors declare no conflicts of interest.

975

976 **References**

- 977 Allam, A. A., Kroll, K. A., Milliner, C. W. D., and Richards-Dinger, K. B.: Effects of Fault  
978 Roughness on Coseismic Slip and Earthquake Locations, *Journal of Geophysical Research:*  
979 *Solid Earth*, 124, 11336–11349, <https://doi.org/10.1029/2018JB016216>, 2019.
- 980 Anderson, H. and Jackson, J.: Active tectonics of the Adriatic Region, *Geophysical Journal of*  
981 *the Royal Astronomical Society*, 91, 937–983, [https://doi.org/10.1111/j.1365-  
982 \*246X.1987.tb01675.x\*, 1987.](https://doi.org/10.1111/j.1365-246X.1987.tb01675.x)
- 983 Bagh, S., Chiaraluce, L., De Gori, P., Moretti, M., Govoni, A., Chiarabba, C., Di Bartolomeo,  
984 P., and Romanelli, M.: Background seismicity in the Central Apennines of Italy: The Abruzzo  
985 region case study, *Tectonophysics*, 444, 80–92, <https://doi.org/10.1016/j.tecto.2007.08.009>,  
986 2007.
- 987 Barbot, S.: Slow-slip, slow earthquakes, period-two cycles, full and partial ruptures, and  
988 deterministic chaos in a single asperity fault, *Tectonophysics*, 768, 228171,  
989 <https://doi.org/10.1016/j.tecto.2019.228171>, 2019.
- 990 Bello, S., Lavecchia, G., Andrenacci, C., Ercoli, M., Cirillo, D., Carboni, F., Barchi, M. R., and  
991 Brozzetti, F.: Complex trans-ridge normal faults controlling large earthquakes, *Sci Rep*, 12,  
992 10676, <https://doi.org/10.1038/s41598-022-14406-4>, 2022.
- 993 Benedetti, L., Tapponnier, P., King, G. c. p., and Piccardi, L.: Surface Rupture of the 1857  
994 Southern Italian Earthquake?, *Terra Nova*, 10, 206–210, [https://doi.org/10.1046/j.1365-  
995 \*3121.1998.00189.x\*, 1998.](https://doi.org/10.1046/j.1365-3121.1998.00189.x)
- 996 Benedetti, L., Manighetti, I., Gaudemer, Y., Finkel, R., Malavieille, J., Pou, K., Arnold, M.,  
997 Aumaitre, G., Bourlès, D., and Keddadouche, K.: Earthquake synchrony and clustering on  
998 Fucino faults (Central Italy) as revealed from in situ <sup>36</sup>Cl exposure dating, *Journal of*  
999 *Geophysical Research: Solid Earth*, 118, 4948–4974, <https://doi.org/10.1002/jgrb.50299>, 2013.
- 1000 Bernard, P. and Zollo, A.: The Irpinia (Italy) 1980 earthquake: Detailed analysis of a complex  
1001 normal faulting, *Journal of Geophysical Research: Solid Earth*, 94, 1631–1647,  
1002 <https://doi.org/10.1029/JB094iB02p01631>, 1989.
- 1003 Boschi, E., Gasperini, P., and Mulargia, F.: Forecasting where larger crustal earthquakes are  
1004 likely to occur in Italy in the near future, *Bulletin of the Seismological Society of America*, 85,  
1005 1475–1482, <https://doi.org/10.1785/BSSA0850051475>, 1995.
- 1006 Bradley, A. M.: Software for Efficient Static Dislocation–Traction Calculations in Fault  
1007 Simulators, *Seismological Research Letters*, 85, 1358–1365,  
1008 <https://doi.org/10.1785/0220140092>, 2014.
- 1009 Castelli, V., Galli, P., Camassi, R., and Caracciolo, C.: The 1561 earthquake (s) in Southern  
1010 Italy: new insights into a complex seismic sequence, *Journal of Earthquake Engineering*, 12,  
1011 1054–1077, <https://doi.org/10.1080/13632460801890356>, 2008.
- 1012 Cattania, C.: Complex Earthquake Sequences On Simple Faults, *Geophysical Research Letters*,  
1013 46, 10384–10393, <https://doi.org/10.1029/2019GL083628>, 2019.

- 1014 Cattania, C. and Segall, P.: Crack Models of Repeating Earthquakes Predict Observed  
 1015 Moment-Recurrence Scaling, *Journal of Geophysical Research: Solid Earth*, 124, 476–503,  
 1016 <https://doi.org/10.1029/2018JB016056>, 2019.
- 1017 Cavinato, G. P. and Celles, P. G. D.: Extensional basins in the tectonically bimodal central  
 1018 Apennines fold-thrust belt, Italy: Response to corner flow above a subducting slab in retrograde  
 1019 motion, *Geology*, 27, 955–958, [https://doi.org/10.1130/0091-7613\(1999\)027%253C0955:EBITB%253E2.3.CO;2](https://doi.org/10.1130/0091-7613(1999)027%253C0955:EBITB%253E2.3.CO;2), 1999.
- 1021 Cello, G., Tondi, E., Micarelli, L., and Mattioni, L.: Active tectonics and earthquake sources  
 1022 in the epicentral area of the 1857 Basilicata earthquake (southern Italy), *Journal of*  
 1023 *Geodynamics*, 36, 37–50, [https://doi.org/10.1016/S0264-3707\(03\)00037-1](https://doi.org/10.1016/S0264-3707(03)00037-1), 2003.
- 1024 Chan, C.-H., Sørensen, M. B., Stromeyer, D., Grünthal, G., Heidbach, O., Hakimhashemi, A.,  
 1025 and Catalli, F.: Forecasting Italian seismicity through a spatio-temporal physical model:  
 1026 importance of considering time-dependency and reliability of the forecast, *Annals of*  
 1027 *Geophysics*, 53, 129–140, <https://doi.org/10.4401/ag-4761>, 2010.
- 1028 Chiarabba, C., Jovane, L., and DiStefano, R.: A new view of Italian seismicity using 20 years  
 1029 of instrumental recordings, *Tectonophysics*, 395, 251–268,  
 1030 <https://doi.org/10.1016/j.tecto.2004.09.013>, 2005.
- 1031 Chiaraluce, L., Barchi, M., Collettini, C., Mirabella, F., and Pucci, S.: Connecting seismically  
 1032 active normal faults with Quaternary geological structures in a complex extensional  
 1033 environment: The Colfiorito 1997 case history (northern Apennines, Italy), *Tectonics*, 24,  
 1034 <https://doi.org/10.1029/2004TC001627>, 2005.
- 1035 Chiaraluce, L., Michele, M., Waldhauser, F., Tan, Y. J., Herrmann, M., Spallarossa, D., Beroza,  
 1036 G. C., Cattaneo, M., Chiarabba, C., De Gori, P., Di Stefano, R., Ellsworth, W., Main, I.,  
 1037 Mancini, S., Margheriti, L., Marzocchi, W., Meier, M.-A., Scafidi, D., Schaff, D., and Segou,  
 1038 M.: A comprehensive suite of earthquake catalogues for the 2016-2017 Central Italy seismic  
 1039 sequence, *Sci Data*, 9, 710, <https://doi.org/10.1038/s41597-022-01827-z>, 2022.
- 1040 Cinque, A., Ascione, A., and Caiazzo, C.: Distribuzione spazio-temporale e caratterizzazione  
 1041 della fagliazione quaternaria in Appennino meridionale., *ITA*, 2000.
- 1042 Cowie, P. A., Roberts, G. P., Bull, J. M., and Visini, F.: Relationships between fault geometry,  
 1043 slip rate variability and earthquake recurrence in extensional settings, *Geophysical Journal*  
 1044 *International*, 189, 143–160, <https://doi.org/10.1111/j.1365-246X.2012.05378.x>, 2012.
- 1045 Cowie, P. A., Phillips, R. J., Roberts, G. P., McCaffrey, K., Zijerveld, L. J. J., Gregory, L. C.,  
 1046 Faure Walker, J., Wedmore, L. N. J., Dunai, T. J., Binnie, S. A., Freeman, S. P. H. T., Wilcken,  
 1047 K., Shanks, R. P., Huismans, R. S., Papanikolaou, I., Michetti, A. M., and Wilkinson, M.:  
 1048 Orogen-scale uplift in the central Italian Apennines drives episodic behaviour of earthquake  
 1049 faults, *Sci Rep*, 7, 44858, <https://doi.org/10.1038/srep44858>, 2017.
- 1050 D’Addezio, G., Pantosti, G., and Valensise, G.: Paleoearthquakes along the Irpinia fault at  
 1051 Pantano di San Gregorio Magno (southern Italy), *Alpine and Mediterranean Quaternary*, 4,  
 1052 121–136, 1991.
- 1053 Delogkos, E., Howell, A., Seebeck, H., Shaw, B. E., Nicol, A., Mika Liao, Y.-W., and Walsh,  
 1054 J. J.: Impact of Variable Fault Geometries and Slip Rates on Earthquake Catalogs From

- 1055 Physics-Based Simulations of a Normal Fault, *Journal of Geophysical Research: Solid Earth*,  
1056 128, e2023JB026746, <https://doi.org/10.1029/2023JB026746>, 2023.
- 1057 Dieterich, J. H.: Modeling of rock friction I. Experimental results and constitutive equations,  
1058 *Journal of Geophysical Research: Solid Earth*, 84, 2161–2168,  
1059 <https://doi.org/10.1029/JB084iB05p02161>, 1979.
- 1060 Dieterich, J. H. and Richards-Dinger, K. B.: Earthquake Recurrence in Simulated Fault  
1061 Systems, *Pure Appl. Geophys.*, 167, 1087–1104, <https://doi.org/10.1007/s00024-010-0094-0>,  
1062 2010.
- 1063 Dieterich, J. H. and Smith, D. E.: Nonplanar Faults: Mechanics of Slip and Off-fault Damage,  
1064 in: *Mechanics, Structure and Evolution of Fault Zones*, edited by: Ben-Zion, Y. and Sammis,  
1065 C., Birkhäuser, Basel, 1799–1815, [https://doi.org/10.1007/978-3-0346-0138-2\\_12](https://doi.org/10.1007/978-3-0346-0138-2_12), 2010.
- 1066 Doglioni, C.: Some remarks on the origin of foredeeps, *Tectonophysics*, 228, 1–20,  
1067 [https://doi.org/10.1016/0040-1951\(93\)90211-2](https://doi.org/10.1016/0040-1951(93)90211-2), 1993.
- 1068 Erickson, B. A., Jiang, J., Barall, M., Lapusta, N., Dunham, E. M., Harris, R., Abrahams, L. S.,  
1069 Allison, K. L., Ampuero, J., Barbot, S., Cattania, C., Elbanna, A., Fialko, Y., Idini, B., Kozdon,  
1070 J. E., Lambert, V., Liu, Y., Luo, Y., Ma, X., Best McKay, M., Segall, P., Shi, P., van den Ende,  
1071 M., and Wei, M.: The Community Code Verification Exercise for Simulating Sequences of  
1072 Earthquakes and Aseismic Slip (SEAS), *Seismological Research Letters*, 91, 874–890,  
1073 <https://doi.org/10.1785/0220190248>, 2020.
- 1074 Faure Walker, J. P.: *Mechanics of continental extension from Quaternary strain fields in the*  
1075 *Italian Apennines*, Doctoral, UCL (University College London), 405 pp., 2010.
- 1076 Faure Walker, J. P., Roberts, G. P., Cowie, P. A., Papanikolaou, I. D., Sammonds, P. R.,  
1077 Michetti, A. M., and Phillips, R. J.: Horizontal strain-rates and throw-rates across breached  
1078 relay zones, central Italy: Implications for the preservation of throw deficits at points of normal  
1079 fault linkage, *Journal of Structural Geology*, 31, 1145–1160,  
1080 <https://doi.org/10.1016/j.jsg.2009.06.011>, 2009.
- 1081 Faure Walker, J. P., Visini, F., Roberts, G., Galasso, C., McCaffrey, K., and Mildon, Z.:  
1082 Variable Fault Geometry Suggests Detailed Fault-Slip-Rate Profiles and Geometries Are  
1083 Needed for Fault-Based Probabilistic Seismic Hazard Assessment (PSHA), *Bulletin of the*  
1084 *Seismological Society of America*, 109, 110–123, <https://doi.org/10.1785/0120180137>, 2019a.
- 1085 Faure Walker, J. P., Visini, F., Roberts, G., Galasso, C., McCaffrey, K., and Mildon, Z.:  
1086 Variable Fault Geometry Suggests Detailed Fault-Slip-Rate Profiles and Geometries Are  
1087 Needed for Fault-Based Probabilistic Seismic Hazard Assessment (PSHA), *Bulletin of the*  
1088 *Seismological Society of America*, 109, 110–123, <https://doi.org/10.1785/0120180137>, 2019b.
- 1089 Faure Walker, J. P., Boncio, P., Pace, B., Roberts, G., Benedetti, L., Scotti, O., Visini, F., and  
1090 Peruzza, L.: Fault2SHA Central Apennines database and structuring active fault data for  
1091 seismic hazard assessment, *Sci Data*, 8, 87, <https://doi.org/10.1038/s41597-021-00868-0>, 2021.
- 1092 Freed, A. M.: Earthquake Triggering by Static, Dynamic, and Postseismic Stress Transfer,  
1093 *Annual Review of Earth and Planetary Sciences*, 33, 335–367,  
1094 <https://doi.org/10.1146/annurev.earth.33.092203.122505>, 2005.

- 1095 Frepoli, A., Maggi, C., Cimini, G. B., Marchetti, A., and Chiappini, M.: Seismotectonic of  
 1096 Southern Apennines from recent passive seismic experiments, *Journal of Geodynamics*, 51,  
 1097 110–124, <https://doi.org/10.1016/j.jog.2010.02.007>, 2011.
- 1098 Galadini, F. and Galli, P.: Paleoseismology related to deformed archaeological remains in the  
 1099 Fucino Plain. Implications for subrecent seismicity in Central Italy, *Annals of Geophysics*, 39,  
 1100 <https://doi.org/10.4401/ag-4025>, 1996.
- 1101 Galadini, F. and Galli, P.: The Holocene paleoearthquakes on the 1915 Avezzano earthquake  
 1102 faults (central Italy): implications for active tectonics in the central Apennines, *Tectonophysics*,  
 1103 308, 143–170, [https://doi.org/10.1016/S0040-1951\(99\)00091-8](https://doi.org/10.1016/S0040-1951(99)00091-8), 1999a.
- 1104 Galadini, F. and Galli, P.: The Holocene paleoearthquakes on the 1915 Avezzano earthquake  
 1105 faults (central Italy): implications for active tectonics in the central Apennines, *Tectonophysics*,  
 1106 308, 143–170, [https://doi.org/10.1016/S0040-1951\(99\)00091-8](https://doi.org/10.1016/S0040-1951(99)00091-8), 1999b.
- 1107 Galli, P.: Recurrence times of central-southern Apennine faults (Italy): Hints from  
 1108 palaeoseismology, *Terra Nova*, 32, 399–407, <https://doi.org/10.1111/ter.12470>, 2020.
- 1109 Galli, P. and Peronace, E.: New paleoseismic data from the Irpinia Fault. A different  
 1110 seismogenic perspective for southern Apennines (Italy), *Earth-Science Reviews*, 136, 175–  
 1111 201, <https://doi.org/10.1016/j.earscirev.2014.05.013>, 2014.
- 1112 Galli, P., Bosi, V., Piscitelli, S., Giocoli, A., and Scionti, V.: Late Holocene earthquakes in  
 1113 southern Apennine: paleoseismology of the Caggiano fault, *Int J Earth Sci (Geol Rundsch)*, 95,  
 1114 855–870, <https://doi.org/10.1007/s00531-005-0066-2>, 2006a.
- 1115 Galli, P., Bosi, V., Piscitelli, S., Giocoli, A., and Scionti, V.: Late Holocene earthquakes in  
 1116 southern Apennine: paleoseismology of the Caggiano fault, *Int J Earth Sci (Geol Rundsch)*, 95,  
 1117 855–870, <https://doi.org/10.1007/s00531-005-0066-2>, 2006b.
- 1118 Galli, P., Galadini, F., and Pantosti, D.: Twenty years of paleoseismology in Italy, *Earth-*  
 1119 *Science Reviews*, 88, 89–117, <https://doi.org/10.1016/j.earscirev.2008.01.001>, 2008.
- 1120 Galli, P., Giaccio, B., Peronace, E., and Messina, P.: Holocene Paleoseismicity and Early–  
 1121 Late Pleistocene Slip Rate on the Sulmona Fault (Central Apennines, Italy), *Bulletin of the*  
 1122 *Seismological Society of America*, 105, 1–13, <https://doi.org/10.1785/0120140029>, 2015.
- 1123 Galli, P., Giaccio, B., Messina, P., and Peronace, E.: Three magnitude 7 earthquakes on a single  
 1124 fault in central Italy in 1400 years, evidenced by new palaeoseismic results, *Terra Nova*, 28,  
 1125 146–154, <https://doi.org/10.1111/ter.12202>, 2016.
- 1126 Galli, P. A. C., Peronace, E., Quadrio, B., and Esposito, G.: Earthquake fingerprints along fault  
 1127 scarps: A case study of the Irpinia 1980 earthquake fault (southern Apennines),  
 1128 *Geomorphology*, 206, 97–106, <https://doi.org/10.1016/j.geomorph.2013.09.023>, 2014.
- 1129 Galvez, P., Somerville, P., Petukhin, A., Ampuero, J.-P., and Peter, D.: Earthquake Cycle  
 1130 Modelling of Multi-segmented Faults: Dynamic Rupture and Ground Motion Simulation of the  
 1131 1992 Mw 7.3 Landers Earthquake, *Pure Appl. Geophys.*, 177, 2163–2179,  
 1132 <https://doi.org/10.1007/s00024-019-02228-x>, 2020.

- 1133 Gasperini, P. and Ferrari, G.: Deriving numerical estimates from descriptive information: the  
 1134 computation of earthquake parameters, *Annals of Geophysics*, 43, [https://doi.org/10.4401/ag-](https://doi.org/10.4401/ag-3670)  
 1135 3670, 2000.
- 1136 Gerstenberger, M. C., Marzocchi, W., Allen, T., Pagani, M., Adams, J., Danciu, L., Field, E.  
 1137 H., Fujiwara, H., Luco, N., Ma, K. -F., Meletti, C., and Petersen, M. D.: Probabilistic Seismic  
 1138 Hazard Analysis at Regional and National Scales: State of the Art and Future Challenges, *Rev.*  
 1139 *Geophys.*, 58, <https://doi.org/10.1029/2019RG000653>, 2020.
- 1140 Giardini, D., Basili, A., and Boschi, E.: Applying the relative hypocentre location approach:  
 1141 where was the 1980 November 23 Irpinia earthquake?, *Geophysical Journal International*, 127,  
 1142 605–615, <https://doi.org/10.1111/j.1365-246X.1996.tb04041.x>, 1996.
- 1143 Gioia, D., Schiattarella, M., Mattei, M., and Nico, G.: Quantitative morphotectonics of the  
 1144 Pliocene to Quaternary Auletta basin, southern Italy, *Geomorphology*, 134, 326–343,  
 1145 <https://doi.org/10.1016/j.geomorph.2011.07.009>, 2011.
- 1146 Guidoboni, E., Ferrari, G., Tarabusi, G., Sgattoni, G., Comastri, A., Mariotti, D., Ciuccarelli,  
 1147 C., Bianchi, M. G., and Valensise, G.: CFTI5Med, the new release of the catalogue of strong  
 1148 earthquakes in Italy and in the Mediterranean area, *Sci Data*, 6, 80,  
 1149 <https://doi.org/10.1038/s41597-019-0091-9>, 2019.
- 1150 Hanks, T. C. and Kanamori, H.: A moment magnitude scale, *J. Geophys. Res.*, 84, 2348–2350,  
 1151 <https://doi.org/10.1029/JB084iB05p02348>, 1979.
- 1152 Harris, R. A. and Simpson, R. W.: Suppression of large earthquakes by stress shadows: A  
 1153 comparison of Coulomb and rate-and-state failure, *Journal of Geophysical Research: Solid*  
 1154 *Earth*, 103, 24439–24451, <https://doi.org/10.1029/98JB00793>, 1998.
- 1155 Heimisson, E. R.: Crack to pulse transition and magnitude statistics during earthquake cycles  
 1156 on a self-similar rough fault, *Earth and Planetary Science Letters*, 537, 116202,  
 1157 <https://doi.org/10.1016/j.epsl.2020.116202>, 2020.
- 1158 Herrero-Barbero, P., Álvarez-Gómez, J. A., Williams, C., Villamor, P., Insua-Arévalo, J. M.,  
 1159 Alonso-Henar, J., and Martínez-Díaz, J. J.: Physics-Based Earthquake Simulations in Slow-  
 1160 Moving Faults: A Case Study From the Eastern Betic Shear Zone (SE Iberian Peninsula),  
 1161 *Journal of Geophysical Research: Solid Earth*, 126, e2020JB021133,  
 1162 <https://doi.org/10.1029/2020JB021133>, 2021.
- 1163 Hillers, G., Mai, P. M., Ben-Zion, Y., and Ampuero, J.-P.: Statistical properties of seismicity  
 1164 of fault zones at different evolutionary stages, *Geophysical Journal International*, 169, 515–  
 1165 533, <https://doi.org/10.1111/j.1365-246X.2006.03275.x>, 2007.
- 1166 Iacoletti, S., Cremen, G., and Galasso, C.: Advancements in multi-rupture time-dependent  
 1167 seismic hazard modeling, including fault interaction, *Earth-Science Reviews*, 220, 103650,  
 1168 <https://doi.org/10.1016/j.earscirev.2021.103650>, 2021.
- 1169 Jiang, J., Erickson, B. A., Lambert, V. R., Ampuero, J.-P., Ando, R., Barbot, S. D., Cattania,  
 1170 C., Zilio, L. D., Duan, B., Dunham, E. M., Gabriel, A.-A., Lapusta, N., Li, D., Li, M., Liu, D.,  
 1171 Liu, Y., Ozawa, S., Pranger, C., and van Dinther, Y.: Community-Driven Code Comparisons  
 1172 for Three-Dimensional Dynamic Modeling of Sequences of Earthquakes and Aseismic Slip,

- 1173 Journal of Geophysical Research: Solid Earth, 127, e2021JB023519,  
1174 <https://doi.org/10.1029/2021JB023519>, 2022.
- 1175 Jolivet, L., Faccenna, C., Goffé, B., Mattei, M., Rossetti, F., Brunet, C., Storti, F., Funicello,  
1176 R., Cadet, J. P., d'Agostino, N., and Parra, T.: Midcrustal shear zones in postorogenic  
1177 extension: Example from the northern Tyrrhenian Sea, Journal of Geophysical Research: Solid  
1178 Earth, 103, 12123–12160, <https://doi.org/10.1029/97JB03616>, 1998.
- 1179 King, G. C. P., Stein, R. S., and Lin, J.: Static stress changes and the triggering of earthquakes,  
1180 Bulletin of the Seismological Society of America, 84, 935–953,  
1181 <https://doi.org/10.1785/BSSA0840030935>, 1994.
- 1182 Lapusta, N., Rice, J. R., Ben-Zion, Y., and Zheng, G.: Elastodynamic analysis for slow tectonic  
1183 loading with spontaneous rupture episodes on faults with rate- and state-dependent friction,  
1184 Journal of Geophysical Research: Solid Earth, 105, 23765–23789,  
1185 <https://doi.org/10.1029/2000JB900250>, 2000.
- 1186 Lombardi, A. M., Cinti, F. R., and Pantosti, D.: Paleoearthquakes modelling and effects of  
1187 uncertainties on probability assessment of next fault ruptures: the case of Central Italy surface  
1188 faulting earthquakes, Geophysical Journal International, 241, 1327–1347,  
1189 <https://doi.org/10.1093/gji/ggaf105>, 2025.
- 1190 Luo, Y. and Ampuero, J.-P.: Stability of faults with heterogeneous friction properties and  
1191 effective normal stress, Tectonophysics, 733, 257–272,  
1192 <https://doi.org/10.1016/j.tecto.2017.11.006>, 2018.
- 1193 Luo, Y., Ampuero, J. P., Galvez, P., Ende, M. van den, and Idini, B.: QDYN: a Quasi-  
1194 DYNamic earthquake simulator (v1.1), , <https://doi.org/10.5281/zenodo.322459>, 2017.
- 1195 Marone, C.: Laboratory-Derived Friction Laws and Their Application to Seismic Faulting,  
1196 Annual Review of Earth and Planetary Sciences, 26, 643–696,  
1197 <https://doi.org/10.1146/annurev.earth.26.1.643>, 1998a.
- 1198 Marone, C.: The effect of loading rate on static friction and the rate of fault healing during the  
1199 earthquake cycle, Nature, 391, 69–72, <https://doi.org/10.1038/34157>, 1998b.
- 1200 Marturano, A.: The January 15, 1466 and November 23, 1980 Irpinia (Italy) earthquakes,  
1201 Bollettino di Geofisica Teorica ed Applicata, 48, 115–126, 2007.
- 1202 Michetti, A. M., Brunamonte, F., Serva, L., and Vittori, E.: Trench investigations of the 1915  
1203 Fucino earthquake fault scarps (Abruzzo, central Italy): Geological evidence of large historical  
1204 events, Journal of Geophysical Research: Solid Earth, 101, 5921–5936,  
1205 <https://doi.org/10.1029/95JB02852>, 1996.
- 1206 Mignan, A., Danciu, L., and Giardini, D.: Considering large earthquake clustering in seismic  
1207 risk analysis, Nat Hazards, 91, 149–172, <https://doi.org/10.1007/s11069-016-2549-9>, 2018.
- 1208 Mildon, Z. K.: The link between earthquakes and structural geology; the role of elapsed time,  
1209 3D geometry and stress transfer in the central Apennines, Italy, 2017a.
- 1210 Mildon, Z. K.: The link between earthquakes and structural geology; the role of elapsed time,  
1211 3D geometry and stress transfer in the central Apennines, Italy, 2017b.

- 1212 Mildon, Z. K., Roberts, G. P., Faure Walker, J. P., and Toda, S.: Coulomb pre-stress and fault  
1213 bends are ignored yet vital factors for earthquake triggering, *Nat. Commun.*, 1–9,  
1214 <https://doi.org/10.31223/osf.io/pt829>, 2019.
- 1215 Mildon, Z. K., Roberts, G. P., Faure Walker, J. P., Beck, J., Papanikolaou, I., Michetti, A. M.,  
1216 Toda, S., Iezzi, F., Campbell, L., McCaffrey, K. J. W., Shanks, R., Sgambato, C., Robertson,  
1217 J., Meschis, M., and Vittori, E.: Surface faulting earthquake clustering controlled by fault and  
1218 shear-zone interactions, *Nat Commun*, 13, 7126, <https://doi.org/10.1038/s41467-022-34821-5>,  
1219 2022.
- 1220 Milner, K. R., Shaw, B. E., Goulet, C. A., Richards-Dinger, K. B., Callaghan, S., Jordan, T.  
1221 H., Dieterich, J. H., and Field, E. H.: Toward Physics-Based Nonergodic PSHA: A Prototype  
1222 Fully Deterministic Seismic Hazard Model for Southern California, *Bulletin of the*  
1223 *Seismological Society of America*, 111, 898–915, <https://doi.org/10.1785/0120200216>, 2021.
- 1224 Morewood, N. C. and Roberts, G. P.: The geometry, kinematics and rates of deformation within  
1225 an en échelon normal fault segment boundary, central Italy, *Journal of Structural Geology*, 22,  
1226 1027–1047, [https://doi.org/10.1016/S0191-8141\(00\)00030-4](https://doi.org/10.1016/S0191-8141(00)00030-4), 2000.
- 1227 Mouslopoulou, V., Nicol, A., Howell, A., and Griffin, J. D.: Comparison of Paleoearthquake  
1228 Elapsed-Times and Mean Interevent-Times for a Global Data Set of Active Faults: Implications  
1229 for Future Earthquakes and Seismic Hazard, *Journal of Geophysical Research: Solid Earth*,  
1230 130, e2024JB030036, <https://doi.org/10.1029/2024JB030036>, 2025.
- 1231 Nicol, A., Watterson, J., Walsh, J. J., and Childs, C.: The shapes, major axis orientations and  
1232 displacement patterns of fault surfaces, *Journal of Structural Geology*, 18, 235–248,  
1233 [https://doi.org/10.1016/S0191-8141\(96\)80047-2](https://doi.org/10.1016/S0191-8141(96)80047-2), 1996.
- 1234 Nicol, A., Walsh, J., Berryman, K., and Nodder, S.: Growth of a normal fault by the  
1235 accumulation of slip over millions of years, *Journal of Structural Geology*, 27, 327–342,  
1236 <https://doi.org/10.1016/j.jsg.2004.09.002>, 2005.
- 1237 Nicol, A., Robinson, R., Van Dissen, R., and Harvison, A.: Variability of recurrence interval  
1238 and single-event slip for surface-rupturing earthquakes in New Zealand, *New Zealand Journal*  
1239 *of Geology and Geophysics*, 59, 97–116, <https://doi.org/10.1080/00288306.2015.1127822>,  
1240 2016.
- 1241 Okada, Y.: Internal deformation due to shear and tensile faults in a half-space, *Bulletin of the*  
1242 *Seismological Society of America*, 82, 1018–1040, <https://doi.org/10.1785/BSSA0820021018>,  
1243 1992.
- 1244 Pace, B., Visini, F., and Peruzza, L.: *FiSH*: MATLAB Tools to Turn Fault Data into Seismic-  
1245 Hazard Models, *Seismological Research Letters*, 87, 374–386,  
1246 <https://doi.org/10.1785/0220150189>, 2016.
- 1247 Pace, B., Valentini, A., Ferranti, L., Vasta, M., Vassallo, M., Montagna, P., Colella, A., and  
1248 Pons-Branchu, E.: A Large Paleoearthquake in the Central Apennines, Italy, Recorded by the  
1249 Collapse of a Cave Speleothem, *Tectonics*, 39, e2020TC006289,  
1250 <https://doi.org/10.1029/2020TC006289>, 2020.
- 1251 Pantosti, D., Schwartz, D. P., and Valensise, G.: Paleoseismology along the 1980 surface  
1252 rupture of the Irpinia Fault: Implications for earthquake recurrence in the southern Apennines,

- 1253 Italy, *Journal of Geophysical Research: Solid Earth*, 98, 6561–6577,  
1254 <https://doi.org/10.1029/92JB02277>, 1993.
- 1255 Papanikolaou, I. D. and Roberts, G. P.: Geometry, kinematics and deformation rates along the  
1256 active normal fault system in the southern Apennines: Implications for fault growth, *Journal of*  
1257 *Structural Geology*, 29, 166–188, <https://doi.org/10.1016/j.jsg.2006.07.009>, 2007.
- 1258 Papanikolaou, I. D., Roberts, G. P., and Michetti, A. M.: Fault scarps and deformation rates in  
1259 Lazio–Abruzzo, Central Italy: Comparison between geological fault slip-rate and GPS data,  
1260 *Tectonophysics*, 408, 147–176, <https://doi.org/10.1016/j.tecto.2005.05.043>, 2005.
- 1261 Pizzi, A., Falcucci, E., Gori, S., Galadini, F., Messina, P., Vincenzo, M., Giaccio, B., Pomposo,  
1262 G., and Sposato, A.: Active faulting in the Maiella Massif (central Apennines, Italy), *GeoActa*  
1263 *Special Publication*, 3, 2010.
- 1264 QGIS Development Team: QGIS Geographic Information System, Open Source Geospatial  
1265 Foundation, 2009.
- 1266 Rice, J. R.: Spatio-temporal complexity of slip on a fault, *Journal of Geophysical Research:*  
1267 *Solid Earth*, 98, 9885–9907, <https://doi.org/10.1029/93JB00191>, 1993.
- 1268 Rice, J. R. and Ben-Zion, Y.: Slip complexity in earthquake fault models., *Proceedings of the*  
1269 *National Academy of Sciences*, 93, 3811–3818, <https://doi.org/10.1073/pnas.93.9.3811>, 1996.
- 1270 Roberts, G. P.: Fault orientation variations along the strike of active normal fault systems in  
1271 Italy and Greece: Implications for predicting the orientations of subseismic-resolution faults in  
1272 hydrocarbon reservoirs, *Bulletin*, 91, 1–20, <https://doi.org/10.1306/08300605146>, 2007.
- 1273 Roberts, G. P. and Michetti, A. M.: Spatial and temporal variations in growth rates along active  
1274 normal fault systems: an example from The Lazio–Abruzzo Apennines, central Italy, *Journal*  
1275 *of Structural Geology*, 26, 339–376, [https://doi.org/10.1016/S0191-8141\(03\)00103-2](https://doi.org/10.1016/S0191-8141(03)00103-2), 2004.
- 1276 Roberts, G. P., Sgambato, C., Mildon, Z. K., Iezzi, F., Beck, J., Robertson, J., Papanikolaou,  
1277 I., Michetti, A. M., Faure Walker, J. P., Meschis, M., Shanks, R., Phillips, R., McCaffrey, K.  
1278 J. W., Vittori, E., and Mitchell, S.: Spatial migration of temporal earthquake clusters driven by  
1279 the transfer of differential stress between neighbouring fault/shear-zone structures, *Journal of*  
1280 *Structural Geology*, 181, 105096, <https://doi.org/10.1016/j.jsg.2024.105096>, 2024.
- 1281 Roberts, G. P., Iezzi, F., Sgambato, C., Robertson, J., Beck, J., Mildon, Z. K., Papanikolaou,  
1282 I., Michetti, A. M., Faure Walker, J., Mitchell, S., Meschis, M., Shanks, R., Phillips, R.,  
1283 McCaffrey, K., Vittori, E., and Iqbal, M.: Characteristics and modelling of slip-rate variability  
1284 and temporal earthquake clustering across a distributed network of active normal faults  
1285 constrained by in situ <sup>36</sup>Cl cosmogenic dating of fault scarp exhumation, central Italy, *Journal*  
1286 *of Structural Geology*, 195, 105391, 2025.
- 1287 Rodriguez Picada, C., Mildon, Z. K., van den Ende, M., Ampuero, J.-P., and Andrews, B. J.:  
1288 Normal Fault Interactions in Seismic Cycles and the Impact of Fault Network Geometry,  
1289 *Journal of Geophysical Research: Solid Earth*, 130, e2024JB030382,  
1290 <https://doi.org/10.1029/2024JB030382>, 2025a.

1291 Rodriguez Piceda, C., Mildon, Z., Yin, Y., and Galvez, P.: qdyn\_hmat\_lsoda: QDYN  
1292 earthquake simulator with Hierarchical matrices and LSODA solver, ,  
1293 <https://doi.org/10.5281/zenodo.17178002>, 2025b.

1294 Rodriguez Piceda, C., Mildon, Z., Andrews, B. J., Visini, F., Ampuero, J. P., and van den Ende,  
1295 M.: Spatially heterogenous Holocene slip rates drive seismic sequence variability on normal  
1296 faults, *Seismica*, 4, <https://doi.org/10.26443/seismica.v4i2.1682>, 2025c.

1297 Rodriguez Piceda, C., Mildon, Z., Andrews, B., Yin, Y., Ampuero, J. P., van den Ende, M.,  
1298 Sgambato, C., and Galvez, P.: Supplementary information 3D seismic cycle models of the  
1299 Italian Apennines (2), <https://doi.org/10.5281/zenodo.18339858>, 2026.

1300 Romanet, P., Bhat, H. S., Jolivet, R., and Madariaga, R.: Fast and Slow Slip Events Emerge  
1301 Due to Fault Geometrical Complexity, *Geophysical Research Letters*, 45, 4809–4819,  
1302 <https://doi.org/10.1029/2018GL077579>, 2018.

1303 Rovida, A., Locati, M., Camassi, R., Lolli, B., and Gasperini, P.: The Italian earthquake  
1304 catalogue CPTI15, *Bull Earthquake Eng*, 18, 2953–2984, <https://doi.org/10.1007/s10518-020-00818-y>, 2020.

1306 Rubin, A. M. and Ampuero, J.-P.: Earthquake nucleation on (aging) rate and state faults,  
1307 *Journal of Geophysical Research: Solid Earth*, 110, <https://doi.org/10.1029/2005JB003686>,  
1308 2005.

1309 Ruina, A.: Slip instability and state variable friction laws., *Journal of Geophysical Research*,  
1310 88, 10359–10370, <https://doi.org/10.1029/JB088iB12p10359>, 1983.

1311 Savage, J. C.: A dislocation model of strain accumulation and release at a subduction zone, *J.*  
1312 *Geophys. Res.*, 88, 4984–4996, <https://doi.org/10.1029/JB088iB06p04984>, 1983.

1313 Sgambato, C.: Variations in fault parameters and seismic hazard in the Central and Southern  
1314 Italian Apennines, Doctoral, UCL (University College London), 522 pp., 2022.

1315 Sgambato, C., Faure Walker, J. P., Mildon, Z. K., and Roberts, G. P.: Stress loading history of  
1316 earthquake faults influenced by fault/shear zone geometry and Coulomb pre-stress, *Sci Rep*,  
1317 10, 12724, <https://doi.org/10.1038/s41598-020-69681-w>, 2020a.

1318 Sgambato, C., Faure Walker, J. P., and Roberts, G. P.: Uncertainty in strain-rate from field  
1319 measurements of the geometry, rates and kinematics of active normal faults: Implications for  
1320 seismic hazard assessment, *Journal of Structural Geology*, 131, 103934,  
1321 <https://doi.org/10.1016/j.jsg.2019.103934>, 2020b.

1322 Sgambato, C., Faure Walker, J. P., Roberts, G. P., Mildon, Z. K., and Meschis, M.: Influence  
1323 of Fault System Geometry and Slip Rates on the Relative Role of Coseismic and Interseismic  
1324 Stresses on Earthquake Triggering and Recurrence Variability, *Journal of Geophysical*  
1325 *Research: Solid Earth*, 128, e2023JB026496, <https://doi.org/10.1029/2023JB026496>, 2023.

1326 Sgambato, C., Roberts, G. P., Iezzi, F., Faure Walker, J. P., Beck, J., Mildon, Z. K., Michetti,  
1327 A. M., Vittori, E., Robertson, J., Gheorghiu, D. M., and Shanks, R. P.: Millennial Slip-Rates  
1328 Variability of Along-Strike Active Faults in the Italian Southern Apennines Revealed by  
1329 Cosmogenic <sup>36</sup>Cl Dating of Fault Scarps, *Tectonics*, 44, e2024TC008529,  
1330 <https://doi.org/10.1029/2024TC008529>, 2025.

- 1331 Shaw, B. E., Milner, K. R., Field, E. H., Richards-Dinger, K., Gilchrist, J. J., Dieterich, J. H.,  
1332 and Jordan, T. H.: A physics-based earthquake simulator replicates seismic hazard statistics  
1333 across California, *Science Advances*, 4, eaau0688, <https://doi.org/10.1126/sciadv.aau0688>,  
1334 2018.
- 1335 Shaw, B. E., Fry, B., Nicol, A., Howell, A., and Gerstenberger, M.: An Earthquake Simulator  
1336 for New Zealand, *Bulletin of the Seismological Society of America*, 112, 763–778,  
1337 <https://doi.org/10.1785/0120210087>, 2022.
- 1338 Shaw, B. E., Milner, K. R., and Goulet, C. A.: Deterministic Physics-Based Earthquake  
1339 Sequence Simulators Match Empirical Ground-Motion Models and Enable Extrapolation to  
1340 Data-Poor Regimes: Application to Multifault Multimechanism Ruptures, *Seismological  
1341 Research Letters*, 96, 2431–2444, <https://doi.org/10.1785/0220240141>, 2025.
- 1342 Soliva, R., Benedicto, A., Schultz, R. A., Maerten, L., and Micarelli, L.: Displacement and  
1343 interaction of normal fault segments branched at depth: Implications for fault growth and  
1344 potential earthquake rupture size, *Journal of Structural Geology*, 30, 1288–1299,  
1345 <https://doi.org/10.1016/j.jsg.2008.07.005>, 2008.
- 1346 Spagnuolo, E., Herrero, A., and Cultrera, G.: The effect of directivity in a PSHA framework,  
1347 *Geophysical Journal International*, 191, 616–626, [https://doi.org/10.1111/j.1365-  
246X.2012.05630.x](https://doi.org/10.1111/j.1365-<br/>1348 246X.2012.05630.x), 2012.
- 1349 Stein, R. S.: The role of stress transfer in earthquake occurrence, *Nature*, 402, 605–609,  
1350 <https://doi.org/10.1038/45144>, 1999.
- 1351 Stein, R. S., Barka, A. A., and Dieterich, J. H.: Progressive failure on the North Anatolian fault  
1352 since 1939 by earthquake stress triggering, *Geophysical Journal International*, 128, 594–604,  
1353 <https://doi.org/10.1111/j.1365-246X.1997.tb05321.x>, 1997.
- 1354 Thomas, M. Y., Lapusta, N., Noda, H., and Avouac, J.-P.: Quasi-dynamic versus fully dynamic  
1355 simulations of earthquakes and aseismic slip with and without enhanced coseismic weakening,  
1356 *Journal of Geophysical Research: Solid Earth*, 119, 1986–2004,  
1357 <https://doi.org/10.1002/2013JB010615>, 2014.
- 1358 Thompson, E. M. and Worden, C. B.: Estimating Rupture Distances without a Rupture,  
1359 *Bulletin of the Seismological Society of America*, 108, 371–379,  
1360 <https://doi.org/10.1785/0120170174>, 2017.
- 1361 Toda, S., Stein, R. S., Reasenberg, P. A., Dieterich, J. H., and Yoshida, A.: Stress transferred  
1362 by the 1995  $M = 6.9$  Kobe, Japan, shock: Effect on aftershocks and future earthquake  
1363 probabilities, *Journal of Geophysical Research: Solid Earth*, 103, 24543–24565,  
1364 <https://doi.org/10.1029/98JB00765>, 1998.
- 1365 Valentini, A., Visini, F., and Pace, B.: Integrating faults and past earthquakes into a  
1366 probabilistic seismic hazard model for peninsular Italy, *Natural Hazards and Earth System  
1367 Sciences*, 17, 2017–2039, <https://doi.org/10.5194/nhess-17-2017-2017>, 2017.
- 1368 Wells, D. L. and Coppersmith, K. J.: New empirical relationships among magnitude, rupture  
1369 length, rupture width, rupture area, and surface displacement, *Bulletin of the Seismological  
1370 Society of America*, 84, 974–1002, <https://doi.org/10.1785/BSSA0840040974>, 1994.

- 1371 Westaway, R.: Comment [on “Velocity fields in deforming ASia from the inversion of  
1372 earthquake-released strains” by W. E. Holt and A. J. Haines], *Tectonics*, 12, 1485–1488,  
1373 <https://doi.org/10.1029/93TC02252>, 1993a.
- 1374 Westaway, R.: Quaternary uplift of southern Italy, *Journal of Geophysical Research: Solid  
1375 Earth*, 98, 21741–21772, <https://doi.org/10.1029/93JB01566>, 1993b.
- 1376 Westaway, R. and Jackson, J.: The earthquake of 1980 November 23 in Campania—Basilicata  
1377 (southern Italy), *Geophysical Journal International*, 90, 375–443,  
1378 <https://doi.org/10.1111/j.1365-246X.1987.tb00733.x>, 1987.
- 1379 Yin, Y.: *Seismicity and fault interaction through observation and simulation*, ETH Zurich,  
1380 <https://doi.org/10.3929/ETHZ-B-000578638>, 2022.
- 1381 Yin, Y., Galvez, P., Heimisson, E. R., and Wiemer, S.: The role of three-dimensional fault  
1382 interactions in creating complex seismic sequences, *Earth and Planetary Science Letters*, 606,  
1383 118056, <https://doi.org/10.1016/j.epsl.2023.118056>, 2023.
- 1384
- 1385